CELLULAR LOGISTICS
2017, VOL. 7, NO. 3, e1340104 (19 pages)
https://doi.org/10.1080/21592799.2017.1340104

Taylor & Francis
Taylor & Francis Group

RESEARCH PAPER

The ARL2 GTPase regulates mitochondrial fusion from the intermembrane space

Laura E. Newman, Cara R. Schiavon, Rachel E. Turn, and Richard A. Kahn

Department of Biochemistry, Emory University School of Medicine, Atlanta, GA, USA

ABSTRACT

Mitochondria are essential, dynamic organelles that regularly undergo both fusion and fission in response to cellular conditions, though mechanisms of the regulation of their dynamics are incompletely understood. We provide evidence that increased activity of the small GTPase ARL2 is strongly correlated with an increase in fusion, while loss of ARL2 activity results in a decreased rate of mitochondrial fusion. Strikingly, expression of activated ARL2 can partially restore the loss of fusion resulting from deletion of either mitofusin 1 (MFN1) or mitofusin 2 (MFN2), but not deletion of both. We only observe the full effects of ARL2 on mitochondrial fusion when it is present in the intermembrane space (IMS), as constructs driven to the matrix or prevented from entering mitochondria are essentially inactive in promoting fusion. Thus, ARL2 is the first regulatory (small) GTPase shown to act inside mitochondria or in the fusion pathway. Finally, using high-resolution, structured illumination microscopy (SIM), we find that ARL2 and mitofusin immunoreactivities present as punctate staining along mitochondria that share a spatial convergence in fluorescence signals. Thus, we propose that ARL2 plays a regulatory role in mitochondrial fusion, acting from the IMS and requiring at least one of the mitofusins in their canonical role in fusion of the outer membranes.

ARTICLE HISTORY
Received 15 May 2017
Accepted 5 June 2017

KEYWORDS
ADP-ribosylation factor (ARF) like 2; ARL2; cell culture; GTPase; GTPase activating protein (GAP); intermembrane space; membrane fusion; MFN1; MFN2; mitochondria; mitofusin 1; mitofusin 2; SIM; structured illumination microscopy

Introduction

Mitochondria are essential organelles that generate ATP through respiration and play key roles in lipid metabolism, calcium regulation, and apoptosis. They are morphologically heterogeneous and highly dynamic, with the regulation of dynamics playing an integral part in these crucial cellular functions. Mitochondrial shape is regulated by 2 processes, fission and fusion, yet our understanding of the mechanisms and regulation of these processes is incomplete. Central players in these processes are 4 large GTPases: DRP1, MFN1/2, and OPA1. Recruitment of DRP1 from cytosol to the outer membrane is involved in mitochondrial fission.[1,2] Fusion is mediated by the structurally and functionally homologous MFN1 and MFN2, which are transmembrane proteins that promote mitochondrial fusion at the outer membrane. OPA1 is an inner mitochondrial membrane protein that promotes inner membrane fusion.[3-7] The importance of fission and fusion is evident by the number of diseases associated with errors in these processes. Mutations in MFN2 cause Charcot-Marie-Tooth Type 2A,[8] while mutations in OPA1 lead to dominant optic atrophy.[9,10] Mice lacking MFN1 or MFN2 are embryonic lethal,[5] and a conditional knockout of MFN2 leads to defective cerebellar development.[11] In the cell, mitochondrial fusion is important for maintenance of ATP production, and mitochondria elongate during starvation and stress.[12-15] Mitochondrial fusion is important for mixing of mitochondrial contents,[16,17] and maintenance of mitochondrial DNA.[11,18] Thus, better understanding of the mechanisms and means of regulation of mitochondrial dynamics is important to our understanding of cell biology and human diseases.

To date, only a handful of proteins have been shown to regulate fusion, despite the fact that such a pathway is necessary to communicate between the energetic state inside the organelle and external factors, or to link inner and outer mitochondrial membrane events. Bax stimulates mitochondrial fusion via MFN2,[19] and MIB negatively regulates the activity of both mitofusins.[20] In addition, fusogenic activity of OPA1 is regulated by several proteases.[15,21-24] However, more regulators of mitochondrial fusion must exist, given its importance to cell physiology.

ARL2 is a member of the ARF family of regulatory GTPases[25] that is very highly conserved, ubiquitous across eukaryotes, predicted to be present in the last eukaryotic common ancestor,[26] and essential in multiple eukaryotes.[27-29] ARL2 regulates essential functions at several places in the cell. In the cytosol, ARL2 is in a complex with the tubulin folding chaperone cofactor D (TBCD), and together they regulate tubulin folding.[30-33] ARL2 and cofactor D are also at centrosomes, with links to recruitment of γ-tubulin ring complex, tubulin polymerization, and mitotic spindle organization.[34,35] ARL2 can also regulate traffic of farnesylated or N-myristoylated proteins.[36,37] Finally, we have documented roles for ARL2 in mitochondria and the presence of a small pool of cellular ARL2 inside mitochondria.[38,39]

ARL2 only partially localizes to mitochondria, though in a regulated fashion.[39,40] Depletion of ARL2 by siRNA causes 3

CONTACT Prof. Richard A. Kahn rkahn@emory.edu Department of Biochemistry, Emory University School of Medicine, 1510 Clifton Rd, Atlanta, GA 30322, USA.
Supplemental data for this article can be accessed on the publisher's website.

mitochondrial phenotypes: mitochondrial fragmentation, an increase in perinuclear clustering of the organelle, and a dramatic (~50%) loss in cellular ATP.[38] Expression of the dominant negative mutant ARL2[T30N] phenocopied the morphology and motility defects, but not ATP loss, caused by ARL2 siRNA. These observations lead us to propose at least 2 different pathways involving ARL2 in mitochondria: one affecting ATP levels and the other morphology and motility. We extend our previous findings here to document that ARL2 regulates mitochondrial fusion, that it does so from the IMS, and that it displays a highly distinctive staining profile along mitochondria, showing a spatial convergence with mitofusins.

Results

ARL2 regulates mitochondrial fusion

Mitochondrial morphology results from a balance of fission and fusion. Disruption of either of these processes leads to abnormal mitochondrial morphology, with consequences to functions.[3] We previously reported that loss of ARL2 activity, resulting from either siRNA or expression of the dominant inactivating point mutant ARL2[T30N], caused mitochondrial fragmentation in several different cultured cell lines.[38] This fragmentation could be reversed by blocking fission via co-expression with DRP1[K38A], indicating that fusion was occurring in these cells. However, DRP1[K38A] also reversed fragmentation caused by impaired fusion due to the deletion of fusion proteins MFN1 or MFN2[5]. Based on these results, we cannot exclude the possibility that a decrease in the rate of fusion was occurring in ARL2[T30N] expressing cells and causing mitochondrial fragmentation, similar to cells null for MFN1 or MFN2. Therefore, to more directly assess the mechanism by which changes in ARL2 activity affect mitochondrial morphology, we monitored mitochondrial fusion in live cells using mitochondria-targeted photoactivatable GFP (mito-PAGFP), as described previously,[41,42] and under Experimental Procedures. In summary, cells were co-transfected with mito-PAGFP and a mitochondrial marker (mito-dsRed), each of which was efficiently imported into mitochondria. A region of interest (ROI) was then photoactivated, and fluorescence within the entire cell was monitored by live cell imaging for 40 minutes to determine the speed with which the activated mito-PAGFP (green) signal mixed with the mito-dsRed in all mitochondria. A decrease in the rate of spreading of mito-PAGFP fluorescence has been well documented to be a clear indication of a defect in the rate of mitochondrial fusion.[41,42] Cells were co-transfected with mito-PAGFP, mito-dsRed, and either ARL2 or ARL2[T30N]. In cells receiving empty vector or wild type ARL2, the GFP signal was spread throughout the cell within 40 minutes (Fig. 1A). In contrast, expression of ARL2[T30N] resulted in a dramatic loss in the rate of spreading of mito-PAGFP under the same conditions and time frame (Fig. 1A). We quantified the rate of spreading of activated mito-PAGFP by determining the percentage of red (mito-dsRed) pixels that were also green, as described previously.[43,44] The difference in this ratio at 10 min intervals up to 40 minutes after photoactivation is reported as the percent increase in mitochondrial fusion over that seen immediately after photoactivation (Fig. 1B). Cells receiving empty vector or ARL2 had a 30% and 31% increase in mitochondrial fusion, respectively, in agreement with previous reports.[43,44] In contrast, cells expressing ARL2[T30N] showed marked decreases in the rate of fusion at every time point, with only a 13% increase at the last time point (Fig. 2B). These results support the conclusion that expression of ARL2[T30N] results in a loss in the rate of mitochondrial fusion.

In that same study, we also found that ARL2[T30N], along with ARL2 siRNA, caused perinuclear clustering and a loss in plus-end directed mitochondrial motility, in addition to mitochondrial fragmentation, though the loss in motility occurred at later time points (30 hr) than did fragmentation (24 hr).[38] To minimize the effects of mitochondrial motility defects on the mito-PAGFP assay, we excluded from our analyses cells that displayed any hint of perinuclear clustering of mitochondria. To further ensure that mitochondrial motility was not compromised, we also performed the mito-PAGFP assay and imaged cells every 30 seconds, to better observe mitochondrial movement. We observed apparently normal mitochondrial motility in ARL2 and ARL2[T30N] expressing cells (movies s1 and s2), in contrast to the near complete arrest in mitochondrial motility that occurs at later time points, as documented previously.[38] Thus, the decrease in the rate of fusion we observed with ARL2[T30N] does not appear to be secondary to a loss in mitochondrial motility.

Dominant activating and inactivating mutants of ARL2 have opposite effects on mitochondrial morphology

As the loss of ARL2 activity was found to be associated with a net fragmentation of mitochondria, we hypothesized that increasing ARL2 activity would cause an increase in tubulation of the organelle, as a result of increased fusion. Increased mitochondrial fusion is also less commonly observed than is fragmentation,[45] providing stronger support for a specific role in the regulation of mitochondrial morphology. Like other regulatory GTPases, simple overexpression of ARL2 has no discernible phenotypes as it is highly regulated by its activators (guanine nucleotide exchange factors (GEFs) and GTPase activating proteins (GAPs)). Thus, we used wild type ARL2 throughout as a control for effects of protein overexpression. ARL2[Q70L] is homologous to ARF1[Q71L],[46,47] and RAS [Q61L][48-50] in that the loss of the critical glutamine results in several orders of magnitude decreases in GAP-stimulated GTPase activity, with resulting sustained activation of the GTPase. Expression of the dominant activating mutant, ARL2 [Q70L], was found to cause a profound increase in mitochondrial tubulation, as seen in Fig. 2A (bottom panels). Overexpression of wild type ARL2 has no effect on mitochondrial morphology, as cells appear indistinguishable from untransfected cells or those receiving empty vector (Fig. 2A,B). Mitochondria in HeLa cells expressing ARL2[Q70L] displayed obviously longer mitochondria that were also more interconnected (with more branching and looping structures apparent) compared with controls (Fig. 2A). The increased length and interconnectivity made it difficult to locate individual mitochondria in these cells. We found that 19 and 21% of control cells, receiving empty vector or ARL2 respectively, contained

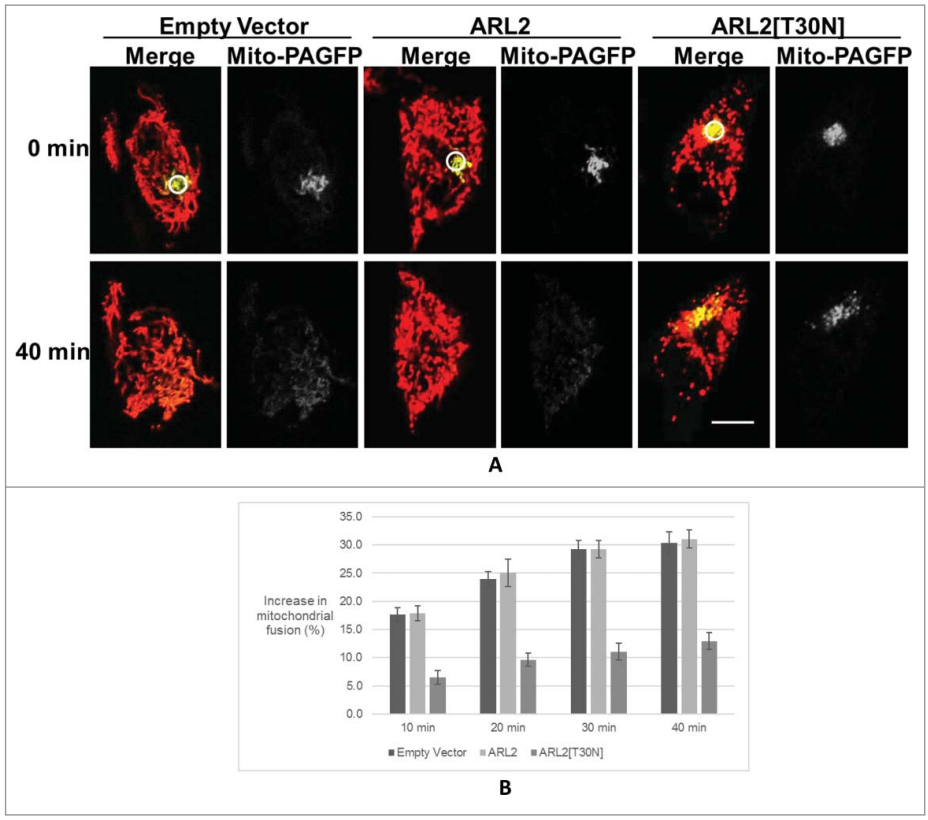

Figure 1. Mitochondrial fusion is impaired in cells expressing ARL2[T30N]. (A) HeLa cells expressing mito-PAGFP (0.5 μg), mito-dsRed (0.25 μg), and either empty vector (left), ARL2 (middle) or ARL2[T30N] (right) (2 μg each) were photoactivated in the ROI shown (white circle, 4 μm diameter; 0 min, top panels), as described under Experimental Procedures. Cells were imaged for up to 40 min (bottom). A single z-plane is shown in each case. Scale bar = 10 μm. Merged images of GFP (green) and dsRed (red) are shown on the left for both conditions, while the GFP channel only (gray) is shown on the right. (B) Mitochondrial fusion was quantified by determining the percentage of pixels within cells that were positive for both green (activated mito-PAGFP) and red (mito-dsRed) signals. The difference in this ratio between 0 min and 10, 20, 30, or 40 min is shown as the percent increase in mitochondrial fusion, as described previously (41–44). N = 15 cells for empty vector, 14 for ARL2 and ARL2[T30N]. Error bars represent standard error of the mean (SEM).

elongated mitochondria, compared with 66% of cells expressing ARL2[Q70L] (Fig. 2B; "elongated").

Unlike the mitochondrial fragmentation caused by ARL2[T30N], which was apparent 24 hours after transfection, mitochondrial elongation caused by ARL2[Q70L] was not obvious until 48 hours after transfection, and was still present 72 hours after transfection. We note that in both ARL2 and ARL2[Q70L] expressing cells ARL2 staining appeared diffuse in the majority of cells the day after transfection, and mitochondrial morphology appeared normal. At later time points, when the mitochondrial elongation phenotype was most apparent in ARL2[Q70L] cells, transfected cells had obviously stronger mitochondrial ARL2 staining. In contrast, mitochondrial staining of ARL2 was clearly increased in cells expressing ARL2[T30N] after just 24 hrs. To further investigate these differences in kinetics, we examined levels of protein expression in whole cell lysates and after crude fractionation of mitochondria at different times after transfection (Fig. 3A,B). Despite the use of the same amount of plasmid DNA and a common expression vector, we found that ARL2[T30N] is present at lower levels than wild type or ARL2[Q70L] (Fig. 3A). This mutation causes reduced affinity for nucleotides, resulting in less stable proteins with shorter half-lives.[51] Interestingly, despite its presence in lower levels in cells, the ARL2[T30N] mutant was found at higher levels than either wild type or ARL2[Q70L] in the 14,000x*g* pellet, which contains the mitochondria. Although not explored further, we speculate that this less stably folded protein may bind with increasing avidity to heat shock proteins that assist in mitochondrial import. Thus, in spite of some differences observed in the kinetics of cellular effects, the dominant activating and inactivating mutants of ARL2 were found to have opposite effects on mitochondrial morphology.

ARL2[Q70L] increases mitochondrial fusion independently of its effects on microtubules

We have previously reported that expression of ARL2[Q70L] also causes microtubule loss.[34] To test the possibility that mitochondrial elongation may be secondary to changes in microtubules, we tested a series of point mutations in ARL2 previously shown to have lost binding to the tubulin co-chaperone cofactor D (TBCD), with consequent loss of effects on microtubules when combined with ARL2[Q70L].[33] This strategy has previously been shown to be highly informative for regulatory GTPases, as key residues in binding to different effectors are often quite different.[52,53] We used structures of ARL2 bound to 2 effectors, BART and PDEδ,[31,54,55] to target residues for mutation. We found 2 point mutations, [L3A] and [F50A,] that had essentially lost all binding to TBCD and effects on microtubules when combined with [Q70L] and expressed in HeLa cells.[33] Despite the loss of effects on microtubules, both ARL2[L3A,Q70L] and ARL2[F50A,Q70L] retained a similar degree of mitochondrial

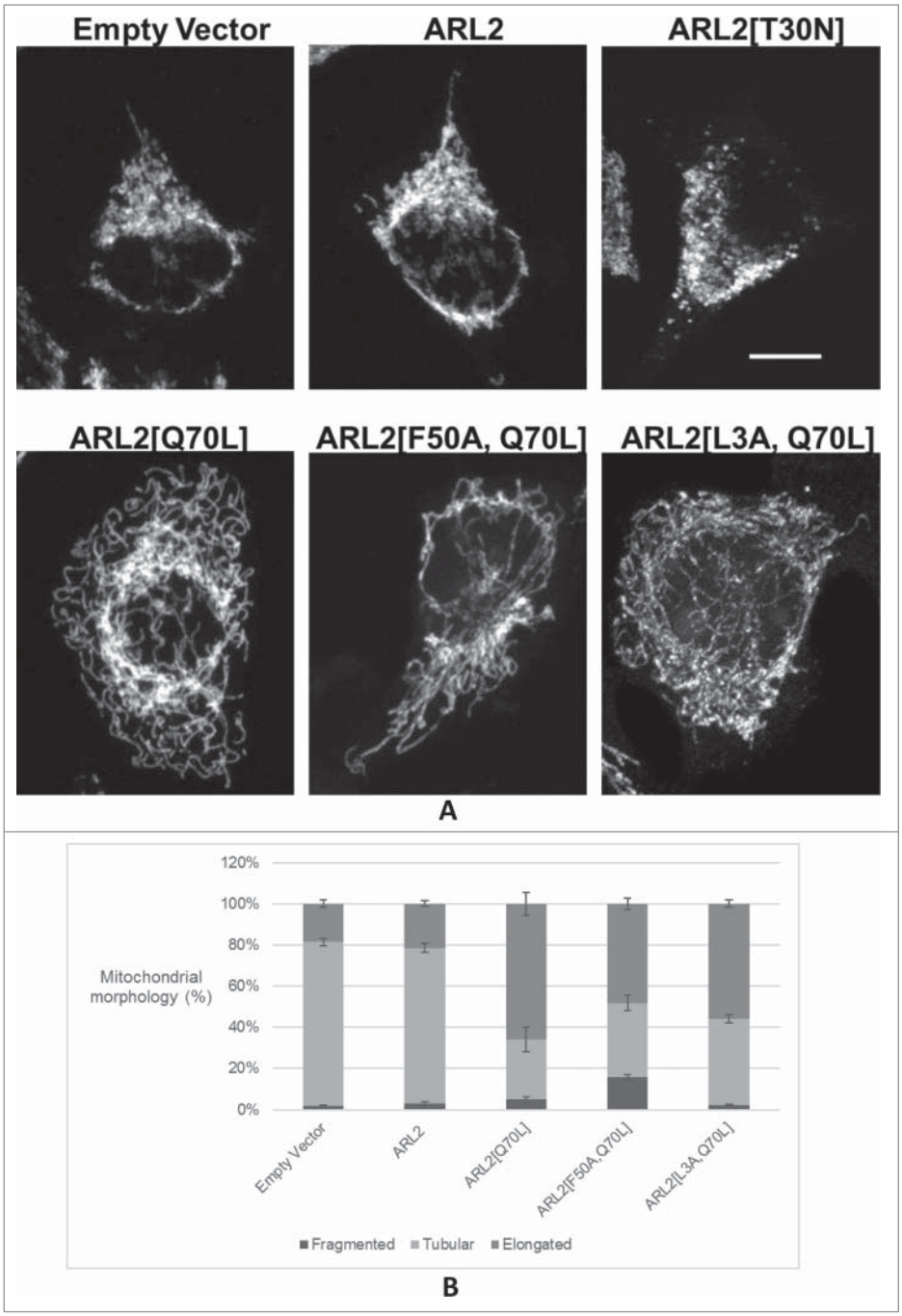

Figure 2. Activating and inactivating mutants of ARL2 have opposing effects on mitochondrial morphology. (A) HeLa cells were transiently transfected with empty vector control (pcDNA3.1) or plasmids (2 μg) directing expression of ARL2, ARL2[T30N], ARL2[Q70L], ARL2[F50A, Q70L], or ARL2[L3A, Q70L]. Cells were fixed 1 day (ARL2[T30N]) or 3 d (all others) after transfection and stained for HSP60, as described under Methods. 2D projections of z-stacks acquired by confocal microscopy are shown, with the exception of the cell expressing ARL2[T30N], where a single z-section is shown. Scale bar = 10 μm. (B) HeLa cells were transiently transfected with ARL2 plasmids, fixed 3 d later, and stained for ARL2 and HSP60. Transfected cells were scored for mitochondrial elongation, as described under Experimental Procedures. N = 625 for empty vector, 606 for ARL2-expressing cells, 601 for ARL2[Q70L], 601 for ARL2[Q70L, F50A], and 600 for ARL2[Q70L, L3A]. For all panels, error bars represent SEM, and the averages from 3 independent experiments are shown.

elongation (56% and 48%, respectively) as the ARL2[Q70L] mutation alone (66%; Fig. 2A,B). Together, these data demonstrate that changes in ARL2 activity in cells correlate with mitochondrial morphology, with more activity linked to elongation and less activity linked to fragmentation, even under conditions in which effects of ARL2 on microtubules were markedly reduced. Results from the use of mitochondrial leader sequences to drive ARL2 proteins inside mitochondria, also without affecting microtubules (see below), further support the conclusion that effects of ARL2 mutants on mitochondrial dynamics cannot be solely the result of indirect effects on microtubules.

ARL2 regulates mitochondrial fusion from the intermembrane space (IMS)

We previously reported that the majority of mitochondria-associated ARL2 localizes to the IMS[39] based upon differential solubilization of purified rat brain mitochondria, though noted

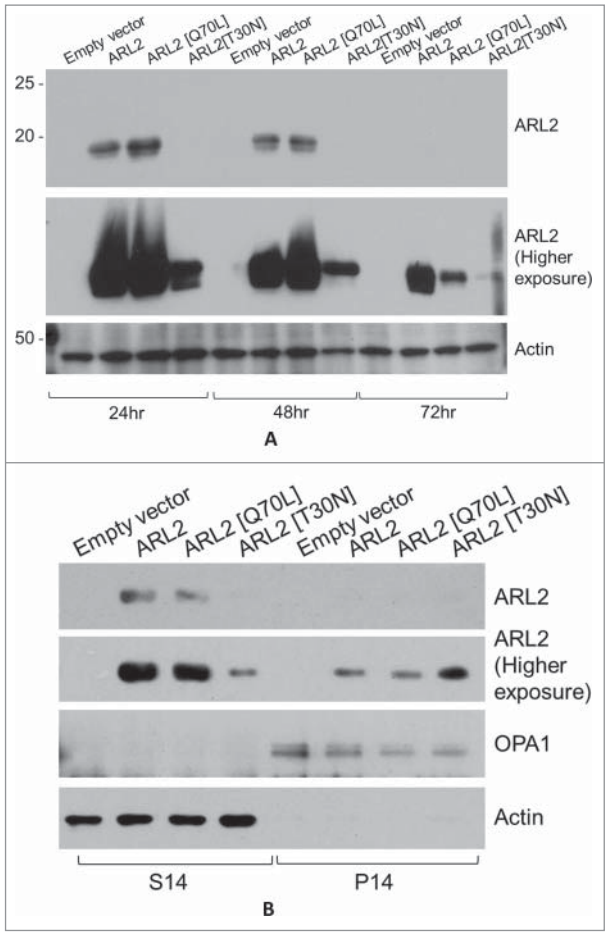

Figure 3. ARL2[T30N] is expressed to lower levels and is less stable than ARL2 or ARL2[Q70L], but a larger fraction is in mitochondria. (A) HeLa cells were transfected with empty vector, or ones driving expression of ARL2, ARL2[Q70L] or ARL2[T30N]. Cells were harvested 24, 48, or 72 hrs later. Lysates (5 μg total protein) were resolved using SDS-PAGE and immunoblotted for ARL2 (top 2 panels) or actin, as a loading control (bottom panel). Overexposure of the ARL2 immunoblot (middle panel) reveals low levels of ARL2[T30N] at each time point, though vanishing amounts at 72 hrs. (B) HeLa cells expressing the same proteins as in (A) at 24 hrs were fractionated as described under Experimental Procedures. Equal volumes of supernatants after centrifugation at 14,000*xg* (S14; lanes 1–4) or pellets (P14; lanes 5–8) were immunoblotted for ARL2 (top 2 panels), OPA1 (mitochondrial marker, middle panel), or actin (cytosolic marker, bottom panel).

its presence also in a pellet that contained matrix proteins. Later we found additional evidence that some ARL2 is present in the matrix, using different concentrations of digitonin to solubilize either the outer or inner membrane of fixed cells, followed by immunofluorescence.[38] To determine its site of action in regulating mitochondrial fusion, we used strong N-terminal leader sequences to direct ARL2 specifically to the IMS or matrix. Each of the 2 mitochondrial localization sequences (MLS) used here have been shown previously to direct fusion proteins to the appropriate site and are cleaved following import, allowing a ready means of monitoring import in immunoblots of whole cell lysates. The MLS from ornithine carbamoyltransferase (OCT, residues 1–32) was used to direct ARL2 proteins to the matrix,[56,57] and the MLS from SMAC/Diablo (SMAC, residues 1–59) was used to direct them to the IMS.[58,59] Each MLS was fused upstream of ARL2, with insertion of an HA epitope tag between the leader and the ARL2 sequences. The generation of these constructs and documentation of their expression and processing upon mitochondrial import have been described recently.[60] The vast majority (estimated at >90% by visual inspection) of OCT-HA-ARL2 and SMAC-HA-ARL2 was determined to be imported, based on their cleavage to a faster migrating species in SDS gels within 24 hours of transfection.[60]

We also took advantage of our observation that addition of even a short (*e.g.*, 9 residue HA) epitope tag to the N-terminus of ARL2 was sufficient to prevent its import into mitochondria. Like other members of the ARF family, the N-terminus of ARL2 forms an amphipathic α helix.[55] While the ARFs are N-myristoylated and their activation is tightly linked to translocation onto a membrane surface, ARL2 is not.[39] Because only a small fraction of total cellular ARL2 is found inside mitochondria, its N-terminus may contain a MLS that is blocked by addition of residues at that end, while addition of the same tag at the C-terminus should not. To test this, we co-expressed either HA-ARL2 or ARL2-HA with mito-GFP in cells. Cells were later briefly (1 minute) permeabilized immediately before fixation to wash out cytosolic ARL2 and facilitate visualization of the mitochondrial pool of ARL2, as described under Experimental Procedures. Following washout, HA staining was clearly observed in cells expressing ARL2-HA, and this staining overlapped extensively with that of mito-GFP (Fig. 4, left panels). In contrast, almost no mitochondrial HA staining was observed in cells expressing HA-ARL2 after washout (Fig. 4, right panels), despite its expression at comparable levels with ARL2-HA. Deletion of the N-terminal 9 residues from ARL2 also prevented mitochondrial import. Together, these data are consistent with the N-terminus of ARL2 containing a mitochondrial import sequence and provide a useful tool for analyzing effects of ARL2 mutants that cannot enter mitochondria.

We determined whether exogenously expressed proteins that are restricted in cellular distribution to the cytosol (HA-ARL2[T30N]), matrix (OCT-HA-ARL2[T30N]), or IMS (SMAC-HA-ARL2[T30N]) were equally capable of causing mitochondrial fragmentation, similar to untagged ARL2 [T30N]. We found that only SMAC-HA-ARL2[T30N] retained

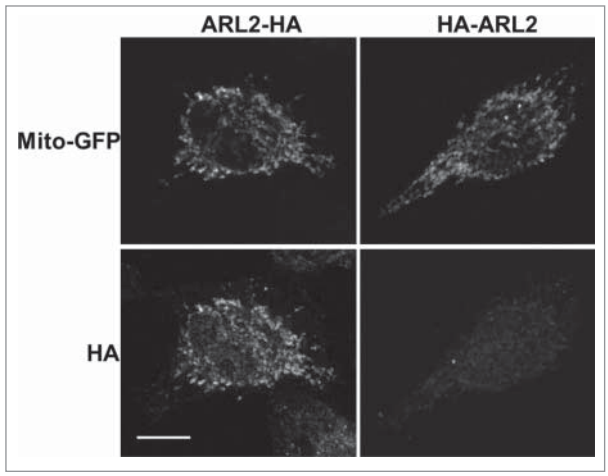

Figure 4. HA-ARL2 is not imported into mitochondria. HeLa cells were co-transfected with mito-GFP and either ARL2-HA or HA-ARL2. Cytosolic staining of overexpressed ARL2 constructs was reduced by permeabilizing cells with 0.05% saponin in PBS for one minute immediately before fixation. Cells were then stained for the HA epitope. Single planes of representative cells are shown and reveal the near complete absence of import of HA-ARL2 into mitochondria (lower right panel). Scale bar = 10 μm.

the ability to fragment mitochondria to a similar extent as untagged ARL2[T30N], as shown in Fig. 5A and quantified in Fig. 5B. Because SMAC-HA-ARL2[T30N] promoted mitochondrial fragmentation, despite retention of the N-terminal HA tag after import and cleavage of the SMAC leader, we conclude that this N-terminal extension did not interfere with ARL2 functions at that location. Expression of SMAC-HA-ARL2[T30N] caused mitochondrial fragmentation in 52% of transfected HeLa cells, compared to 58% of cells expressing untagged ARL2[T30N]. In contrast, expression of ARL2, HA-ARL2, or SMAC-HA-ARL2 had little or no impact on mitochondrial morphology (Fig. 5B), while OCT-HA-ARL2[T30N] had an intermediate effect.

We also used a series of variable strength CMV promoters to drive ARL2 expression, both with and without MLSs.[60] This series of truncations of the CMV promoter, with the largest truncation (CMVΔ6) resulting in the lowest level of expression,[61] allowed us to test effects of protein expression levels. We found CMVΔ6 to express several different proteins to less than ~10% the levels observed with CMVΔ0[60]. Even expression of SMAC-HA-ARL2[T30N] off the weakest promoter (CMVΔ6) caused 43% of cells to have fragmented mitochondria. This is in contrast to controls (empty vector or wild type ARL2), SMAC-ARL2, and HA-ARL2[T30N], which never exceeded 12% of expressing cells to display fragmented mitochondria, even when expressed under the strongest promoter (CMVΔ0). Expression of OCT-HA-ARL2[T30N] also promoted fragmentation, though to only intermediate levels (46%), even with the strongest promoter (Fig. 5B).

A strong preference for IMS localized ARL2[T30N] in causing fragmentation is further supported by the fact that, when expressed off the same promoter (CMVΔ0), SMAC-HA-ARL2 expressed to much lower levels than wild type ARL2 (which was equal to OCT-HA-ARL2)(Fig. 5C, D). Given the strength of the effects seen using IMS targeting promoted by the SMAC MLS and the relative inactivity in this assay of cytosolic or matrix localized proteins, we conclude that ARL2 is most active in regulating mitochondrial morphology from the IMS. We performed similar studies looking at the site of action of ARL2 [Q70L] in promoting fusion but focused on testing this in mouse embryo fibroblasts (MEFs), because of the availability of several invaluable knockout lines (see below).

Fusion defects in MEFs deleted for mitofusins are partially reversed by ARL2[Q70L]

Mitochondrial fusion is mediated by, and dependent upon, 3 large, dynamin-related GTPases. Mitofusins 1 and 2 (MFN1, MFN2) have overlapping roles in outer membrane fusion, and OPA1 regulates inner membrane fusion.[3] While the roles of OPA1 and MFNs can be uncoupled in mammalian cells,[16] a pathway from OPA1 to specifically MFN1 has been proposed.[62] From the IMS, ARL2 has direct access to both mitochondrial membranes so could potentially influence the MFNs, OPA1, or an unknown component in the fusion pathway. To assess the roles of these established modulators of fusion in ARL2 actions and move toward a molecular mechanism for ARL2, we tested for the dependence of ARL2 promoted elongation on MFN1,

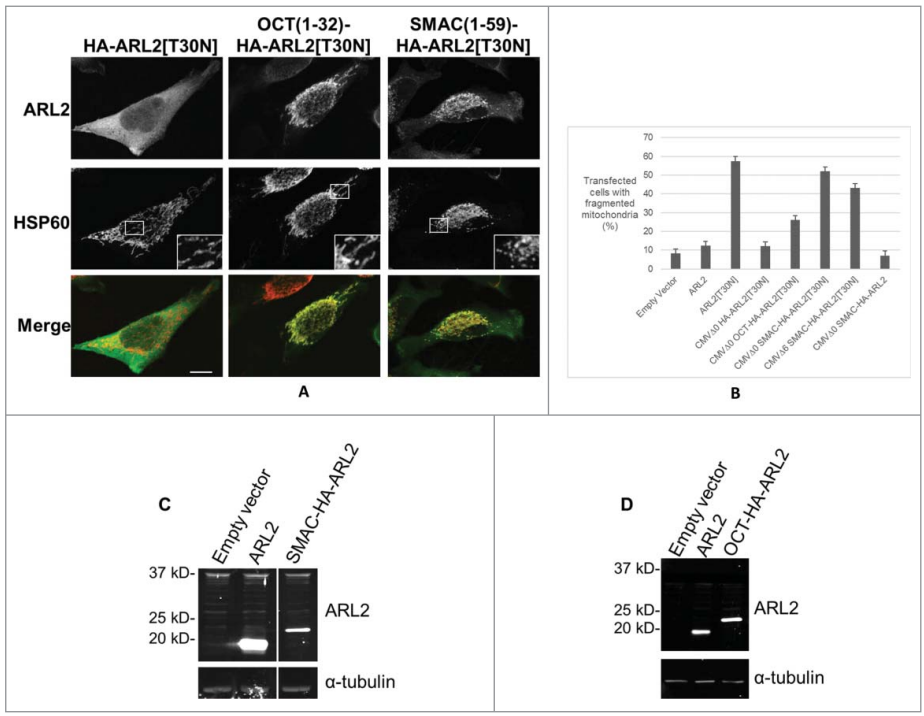

Figure 5. ARL2[T30N] acts from the IMS to fragment mitochondria. (A) HeLa cells were transfected with the indicated plasmid (2 μg), shown along the top, fixed one day after transfection and stained for ARL2 and HSP60. Single planes of representative cells are shown. Insets are 2.5x the size of the larger image shown. Scale bar = 10 μm. (B) Cells treated as described in part A were quantified for mitochondrial fragmentation. The average of 5 experiments is shown, and error bars represent SEM. N = 1035 cells for empty vector, 1005 for ARL2-expressing cells, 1214 for ARL2[T30N], 1023 for OCT(1–32)-HA-ARL2[T30N], 1020 for SMAC(1–59)-HA-ARL2[T30N], 1023 for HA-ARL2 [T30N], 1008 for SMAC(1–59)-HA-ARL2, and 1001 for CMVΔ6 SMAC(1–59)-HA-ARL2[T30N]. (C) HeLa cells were transfected with empty vector, ARL2, or SMAC-HA-ARL2 and lysed 24 hours later. Lysate (20 μg) was immunoblotted for ARL2 and α tubulin, as a loading control. Nonadjacent lanes from the same blot are shown. (D) Same as C, except cells were transfected with OCT-HA-ARL2. All constructs were expressed from the CMVΔ0 promoter, unless stated otherwise.

MFN2, or OPA1. We used the previously characterized, immortalized MEF lines established from *mfn1*$^{-/-}$, *mfn2*$^{-/-}$, *mfn1*$^{-/-}$*mfn2*$^{-/-}$, and *opa1*$^{-/-}$ mice. Each of these displayed fragmented mitochondria due to defective fusion.[4,5,24,63]

Strikingly, expression of ARL2[Q70L] was sufficient to partially reverse the fragmentation of mitochondria resulting from deletion of MFN1 or MFN2, but not when cells have lost both MFNs or OPA1. For these experiments, we used the scoring criteria described under Experimental Procedures (examples shown in Fig. 6I), and as described previously.[19] When *mfn2*$^{-/-}$ MEFs received empty vector, 26% of cells displayed tubular mitochondria – the remaining cells had mitochondria that were completely fragmented (44%) or displayed short tubes that were distinct from the normal, tubular mitochondrial morphology (30%). Expression of ARL2[Q70L] restored tubular morphology in 55% of transfected cells (Fig. 6A, B). In most cells expressing ARL2[Q70L], we saw obviously longer mitochondria that also contained looping structures, similar to what we observed in HeLa cells (compare Fig 2A and Fig. 6A). To exclude effects on microtubules, we also expressed ARL2[F50A, Q70L] in *mfn2*$^{-/-}$ MEFs and found that it also reversed mitochondrial fragmentation (Fig. 7D). Cells overexpressing ARL2 also regained tubular morphology, to a similar extent as cells expressing ARL2[Q70L]. However, ARL2 expressing cells only occasionally displayed elongated mitochondria with looping structures, and typically only in the cells displaying the strongest ARL2 expression (compare Fig. 6A, middle and right panels). The majority of ARL2 expressing cells had a mitochondrial morphology that was similar to that found in wild type MEFs. Though we note the differences between elongated and normal morphology, both were scored as tubular mitochondria in our assay. This effect was transient, as reversal of fragmentation in *mfn2*$^{-/-}$ MEFs was evident at 24 hours post-transfection but was gone by 48 hours.

ARL2[Q70L] was also able to reverse mitochondrial morphology in cells deleted for MFN1, though it did so at somewhat later times after expression. We note that cells lacking MFN1 were more fragmented than those lacking MFN2 and had essentially no tubular mitochondria (compare Fig. 6A and C or quantification in Fig 6B and D). At its peak, 16% of ARL2 [Q70L] expressing *mfn1*$^{-/-}$ MEFs displayed tubular mitochondria, clearly more than the 0% seen with empty vector or 3% in cells overexpressing ARL2 (Fig. 6C, D). The number of cells displaying the intermediate mitochondrial morphology ("short tubes") was also increased (32%), compared with cells receiving empty vector (11%) or expressing ARL2 (18%). Combining these 2 categories, ARL2[Q70L] reduced mitochondrial fragmentation in 48% of transfected cells, compared with 11% of cells receiving empty vector or 21% expressing ARL2 (Fig. 6D). Thus, ARL2[Q70L] approached the ability of MFN2-myc to reverse the fragmentation of mitochondria seen in MEFs deleted for MFN1 (Fig. 6D). To ensure that loss of microtubules was not contributing to the reversal of fragmentation observed in *mfn1*$^{-/-}$ MEFs, we expressed ARL2[F50A, Q70L], which lacks binding to TBCD and effects on microtubules (Fig. 2A) (33), and found that it also promotes mitochondrial elongation to a similar extent as ARL2[Q70L]. This effect was reproducible in repeated experiments and quantified in one representative experiment in which we found that ARL2[F50A, Q70L] and ARL2[Q70L] each caused elongation in 20% of transfected *mfn1*$^{-/-}$ MEFs.

We next asked if ARL2[Q70L] could also reverse fragmentation in the absence of both mitofusins. We obtained lower transfection efficiencies and expression of ARL2 or ARL2 [Q70L] in *mfn1*$^{-/-}$ *mfn2*$^{-/-}$ MEFs. As a result, we needed to use higher laser power to image these cells, resulting in a higher background of cytosolic ARL2 in our images (Fig. 6E). Expression of neither ARL2 nor ARL2[Q70L] reversed the fragmentation at 24, 48, and 51 hours after transfection. In contrast, transient expression of either MFN1-myc or MFN2-myc reversed fragmentation in a large percentage (> 80%) of transfected cells (Fig. 6F).

Expression of ARL2[Q70L] was also unable to reverse fragmentation in cells lacking OPA1. We expressed ARL2 or ARL2 [Q70L] in *opa1*$^{-/-}$ MEFs and found no reversal of fragmentation at either 24 or 48 hours. Similar to *mfn1*$^{-/-}$*mfn2*$^{-/-}$ MEFs, lower expression of ARL2 was observed, so we used higher laser power to image cells (Fig. 6G). In contrast, the transient expression of epitope-tagged OPA1 restored tubular morphology in 46% of transfected cells, and at least partial reversal was seen in another 27% of transfected cells (Fig. 6H). Expression of ARL2[T30N] or ARL2[Q70L] also had no effect upon the proteolytic processing of OPA1 (Fig. 6J), which is linked to its role in fusion.[15,23] Thus, reversal of fragmentation by ARL2[Q70L] requires at least one MFN and OPA1, though it does not appear to act via changes in the processing of OPA1.

Dominant mutants of ARL2 act from the IMS to promote fusion in MEFs

ARL2[T30N] was most active in inhibiting fusion in HeLa cells when targeted to the IMS (Fig. 5A), so we next asked if fusion could also be promoted by ARL2[Q70L] from the same compartment in MEFs. We expressed SMAC-HA-ARL2[Q70L] off of the weakest promoter (CMVΔ6) in *mfn2*$^{-/-}$ MEFs, and observed reversal of fragmentation (Fig. 7A). Due to the low levels of ARL2 expressed, we were unable to identify transfected cells by ARL2 staining. Consequently, we co-expressed GFP to mark transfected cells. When quantified, 47% of GFP expressing cells (also receiving SMAC-HA-ARL2[Q70L]) displayed tubular mitochondria, compared with 27% of GFP expressing cells also receiving empty vector (Fig. 7B). In contrast, OCT-HA-ARL2[Q70L] was unable to increase tubular mitochondria (26%), even when expressed from the strongest (CMVΔ0) promoter. Cytosolic ARL2 (HA-ARL2[Q70L]) was equally ineffective (28%; Fig. 7B). Thus, we conclude that the dominant active mutant of ARL2 promotes fusion in MEFs, acting most effectively when directed to the IMS.

To further ensure that activated ARL2 is increasing fusion in MEFs in a mitofusin-dependent fashion and independent of changes in microtubules, we repeated both testing of microtubule densities and the mitochondrial fusion assays, described above, in *mfn2*$^{-/-}$ MEFs. When cells expressing each construct were stained with antibodies to tubulin, we found that none of them caused the loss of microtubules (Fig. 7C) that is so prominent in cells expressing ARL2[Q70L].[34] Cells receiving empty vector displayed 13% fusion over the 40 min imaging window. In contrast, ARL2 (31%), ARL2[F50A, Q70L] (31%), or

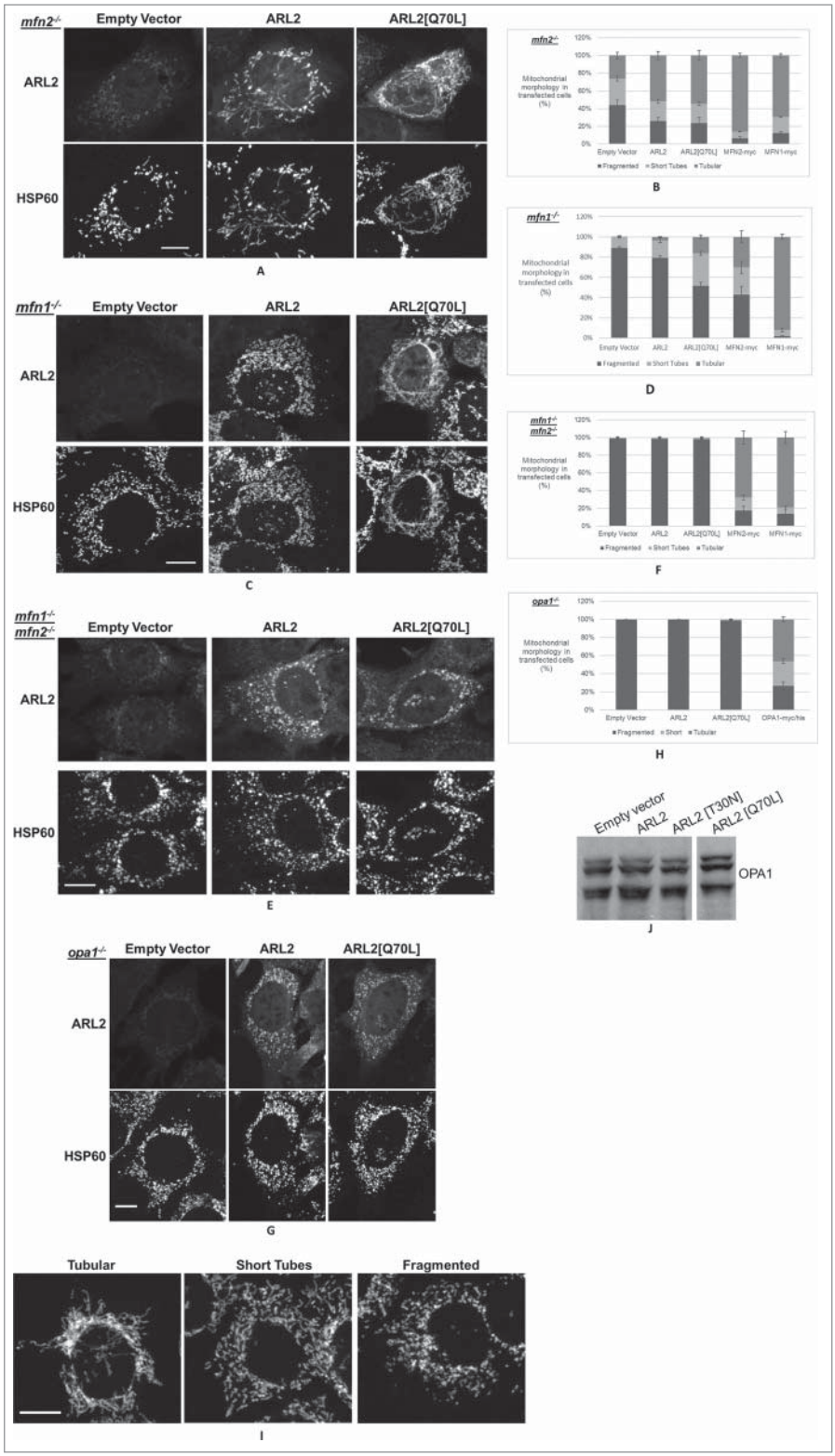

Figure 6. ARL2 or ARL2[Q70L] expression reverses fragmentation in *mfn1*$^{-/-}$ and *mfn2*$^{-/-}$ MEFs. (A) *mfn2*$^{-/-}$ MEFs were transfected with 5 μg empty vector, or the same vector driving expression of ARL2 or ARL2[Q70L], fixed 24 hours later, and stained for ARL2 and HSP60. Note the presence of tubular mitochondria, except in control cells (left panels). (B) Cells treated as described in A were scored for mitochondrial morphology. N = 612 for empty vector, 602 for ARL2 expressing cells, 600 for ARL2[Q70L], 602 for MFN2-myc, 604 for MFN1-myc. (C) Same as in A, except *mfn1*$^{-/-}$ MEFs were transfected, then fixed and stained 51 hours later. (D) Results from C were scored for mitochondrial morphology. N = 622 for empty vector, 614 for ARL2-expressing cells, 607 for ARL2[Q70L], 612 for MFN2-myc, 606 for MFN1-myc. (E) *mfn1*$^{-/-}$ *mfn2*$^{-/-}$ MEFs were treated as described in A, fixed 24 hours later. (F) These cells were then quantified as before; N = 611 for empty vector, 602 for ARL2, 603 for ARL2[Q70L], 609 for MFN2-myc, and 605 for MFN1-myc. (G) *opa1*$^{-/-}$ MEFs were treated as described in A, fixed 24 hours later, and quantified for mitochondrial morphology and shown in (H); N = 620 for empty vector, 606 for ARL2, 603 for ARL2[Q70L], 605 for OPA1-myc/his. (I) Representative cells from the categories used to score mitochondrial morphology in MEFs are shown. Left 2 images are wild type MEFs, right image is a *mfn1*$^{-/-}$ MEF. Scale bar = 10 μm. For all panels, z-stack projections are shown, scale bar = 10 μm, the averages from 3 experiments are shown, with SEM. (J) HeLa cells were transfected with empty vector, ARL2, ARL2[Q70L], or ARL2[T30N]. Cells were harvested one day later and lysates (40 μg) were immunoblotted for OPA1. Nonadjacent lanes from the same blot are shown. No differences in processing of OPA1 were apparent in at least 2 independent experiments.

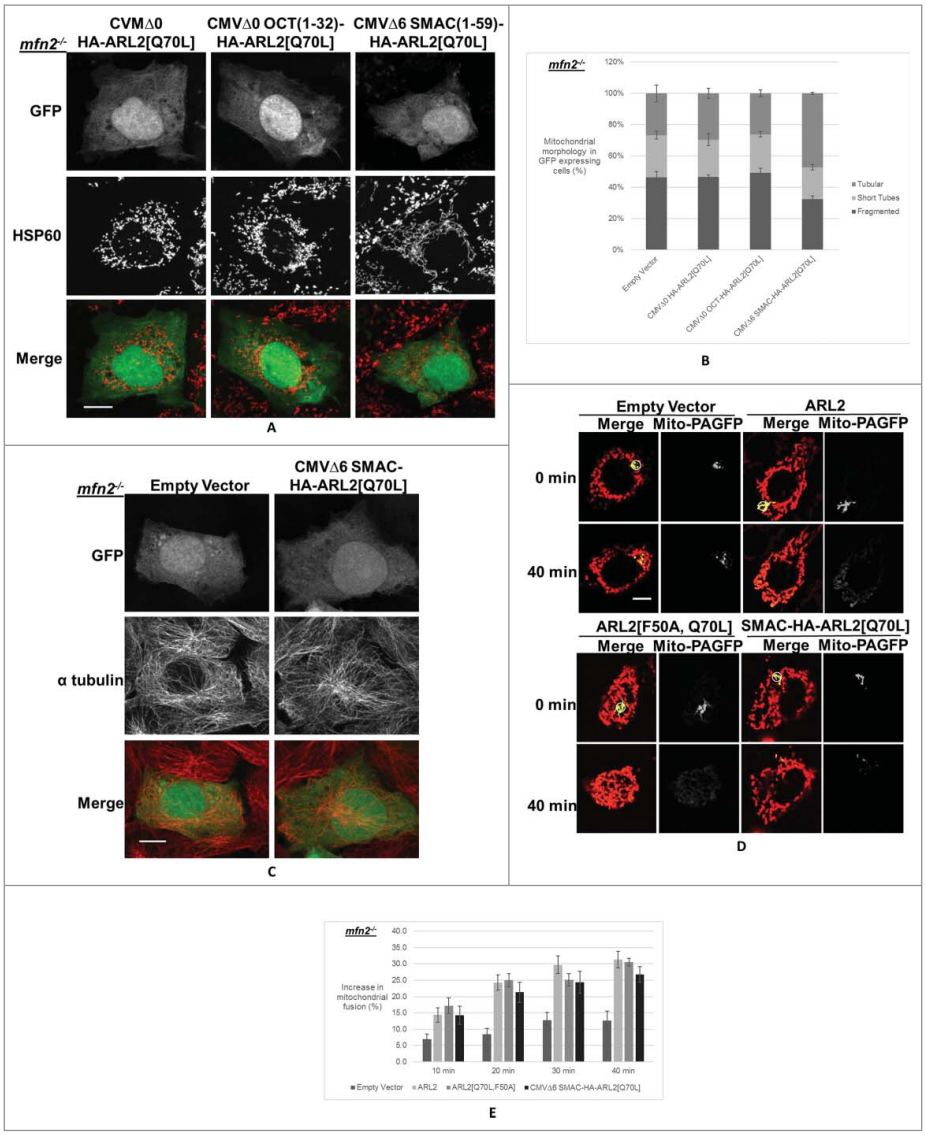

Figure 7. ARL2[Q70L] increases mitochondrial fusion from the IMS in *mfn2*$^{-/-}$ MEFs. (A) *mfn2*$^{-/-}$ MEFs were transfected with GFP (1 μg) and either CMVΔ0 HA-ARL2 [Q70L], CMVΔ0 OCT-HA-ARL2[Q70L], or CMVΔ6 SMAC-HA-ARL2[Q70L] (4 μg). Cells were fixed and stained for HSP60. Z-stack projections are shown. (B) Mitochondrial morphology in GFP expressing cells was scored using the categories shown in Figure 6I. The average of 3 experiments +/− SEM is shown. N = 607 for empty vector, 604 for HA-ARL2[Q70L], and 602 for both CMVΔ0 OCT-HA-ARL2[Q70L] and CMVΔ6 SMAC-HA-ARL2[Q70L]. (C) MEFs were transfected as in (A) and stained for α-tubulin. (D) *mfn2*$^{-/-}$ MEFs expressing mito-PAGFP (2 μg), mito-dsRed (1 μg), and either empty vector (top left), ARL2 (top right), ARL2[F50A, Q70L] (bottom left), or CMVΔ6 SMAC-HA-ARL2[Q70L] (bottom right) (3 μg) were photoactivated in the ROI (white circle; 0 min, top panels), and imaged as described in Figure 1A. A single z-plane is shown in each case. Merged images of GFP (green) and dsRed (red) are shown on the left for both conditions, while the GFP channel only (gray) is shown on the right. Note the slow spread of mito-PAGFP in control cells (top left), consistent with an impaired rate of fusion in *mfn2*$^{-/-}$ MEFs. (E) Results from D were quantified as in Fig. 1B. N = 10 cells for all conditions, with bars indicating SEM. Representative images are shown. All scale bars = 10 μm.

SMAC-HA-ARL2[Q70L] (27%) each promoted more pronounced increases in fusion (Fig. 7D,E). We conclude that ARL2 stimulates fusion in MEFs deleted for MFN2, that it does so acting from the IMS, and that it acts independently of any effects on microtubules.

ARL2 localizes to regularly spaced puncta that display spatial convergence with MFN1/2-myc along mitochondria

In order for increased ARL2 activity in the IMS to reverse fragmentation resulting from the loss of either mitofusin, we posited that it results in increases in the activity of the remaining mitofusin. To begin to explore this model, we asked if ARL2 and mitofusins share physical proximity. Because standard epifluorescence lacks the resolution to distinguish between mitochondrial compartments, we performed structured illumination microscopy (SIM) on cells stained for endogenous ARL2 and mitochondrial proteins. COS7 cells were chosen for these experiments because they are large, flat, and have strong, endogenous, mitochondrial ARL2 staining. We noted earlier that confocal images of endogenous ARL2 in a variety of cultured cells showed mitochondrial staining that was more punctate in appearance than expected for a protein freely diffusible in the IMS.[40] Reconstructions of 3-dimensional SIM images sharpened these differences, and we observed that ARL2 localizes to discrete puncta along mitochondria (Fig. 8A). We noted an evident periodicity to these puncta, so we used ImageJ to perform line scan analyses. This confirmed the periodicity and

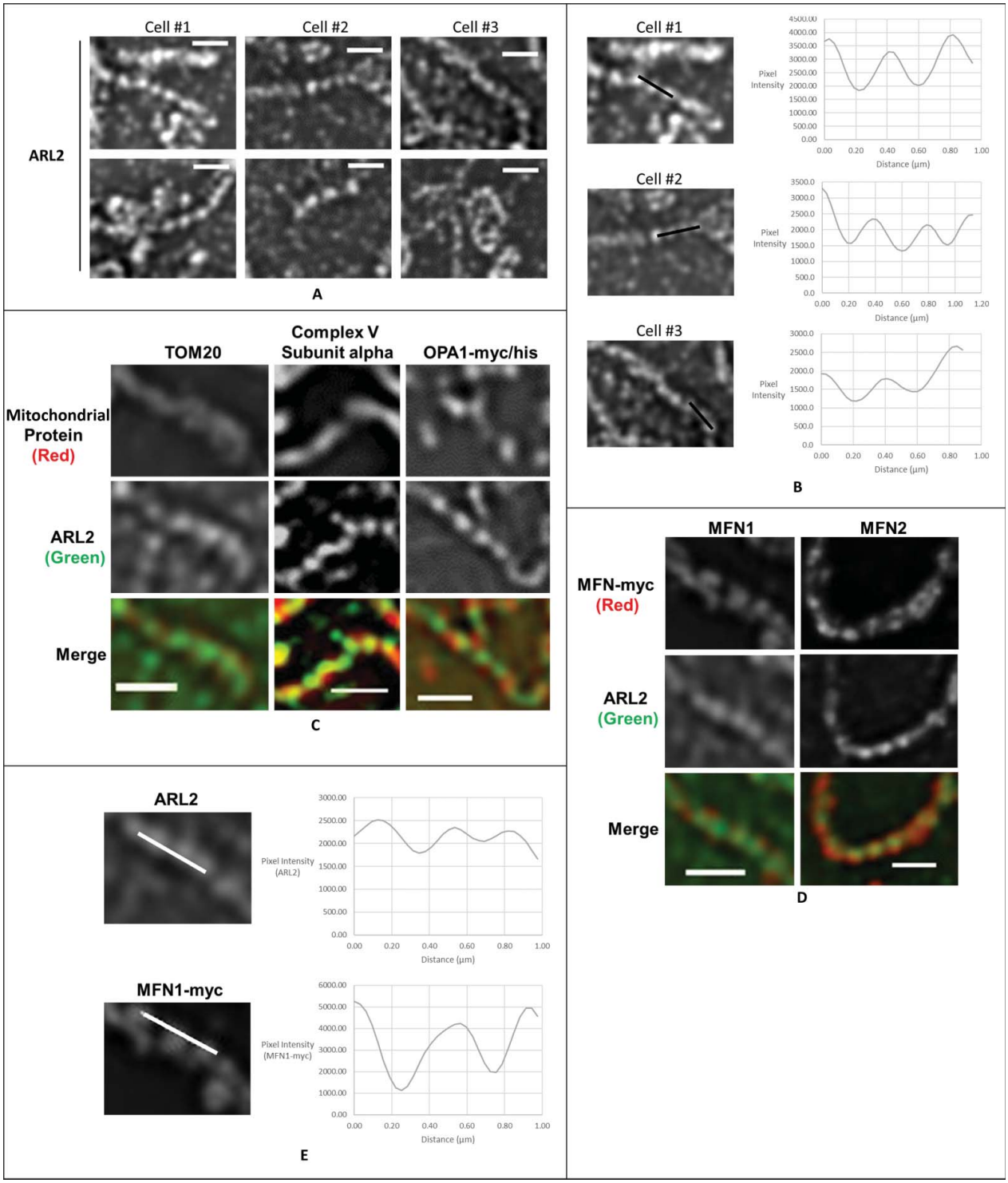

Figure 8. ARL2 localizes to puncta along mitochondria that display regularity in spacing, and mitofusins share these properties. (A) COS7 cells were stained for ARL2 and imaged using 3-dimensional SIM, as described under Experimental Procedures. Two representative examples of mitochondria are shown from each of 3 different cells. (B) Pixel intensity was measured using ImageJ along the lines shown in 3 different cells, revealing that ARL2 puncta repeat at a regular interval of ~0.4 μm. (C) For the left 2 panels, COS7 cells were stained for ARL2 (green) and either TOM20 or Complex V subunit α (red). For the rightmost panel, COS7 cells were transfected with OPA1-myc/his and stained for ARL2 (green) and myc (red). A representative mitochondrion with merged ARL2 and staining for each protein is shown. (D) COS7 cells were transfected with either MFN1–10xmyc or MFN2–16xmyc (0.5 μg), stained for ARL2 and myc, and imaged using 3-dimensional SIM. Myc staining (red) localizes to puncta that align with endogenous ARL2 puncta (green). A representative cell is shown in each case. (E) Line scan analysis from the image shown in D show that MFN1-myc puncta display a similar regularity in spacing as ARL2. All scale bars = 1 μm.

revealed a regularity in spacing of ~0.4 μm (Fig. 8B). These ARL2-positive puncta were also observed in HeLa cells and displayed similar spacing. In this case however, cytosolic ARL2 staining obscured the mitochondrial puncta unless it was removed by cell permeabilization before fixation (data not shown), due to a weaker signal from mitochondrial ARL2 in that cell line. We also observed punctate mitochondrial staining in MEFs, though we found them also more difficult to image compared with COS7 cells, because they are not as flat. ARL2 puncta were evident after fixation with either 2% or 4% PFA, as

well as after permeabilization with either Triton X-100 (0.1%, 10 minutes at room temperature) or methanol (5 minutes at −20). Dual labeling was performed with several mitochondrial markers, including cytochrome c, TOM20, HSP60, a subunit of each of complexes I (NDUFA9), III (UQCRC2), or V (subunit α), DRP1, or mic60/mitophilin. Though each localized to mitochondria, none of the markers showed staining patterns similar to that of ARL2 (TOM20 and complex V subunit α are shown as examples in Fig. 8C). We also examined co-staining with ARL2 after expression of MFF-GFP, DRP1-YFP, or SMAC(1–59)-HA-GFP, and again we found no evidence of spatial convergence in the fluorescence intensities with ARL2 positive puncta. The ARL2 effector BART localizes to mitochondria,[39] and it also appeared as diffuse staining that did not align with ARL2 puncta.

In marked contrast to the negative data for a large number of mitochondrial proteins described above, we found that mitofusins display similarities to ARL2 staining of discrete puncta along mitochondria, with similar spacing and pixel intensities. We were unable to find an antibody to either MFN1 or MFN2 that was useful in such studies, so we expressed C-terminal myc-tagged MFN1/2 (MFN1–10xmyc and MFN2–16xmyc (5)), and stained for myc in fixed COS7 cells. Note that as C-terminal fusions the myc epitopes in these constructs are predicted to reside outside of mitochondria, facing the cytosol.[64] Because overexpression of mitofusins can lead to hyperfusion, perinuclear clustering, and even fragmentation at higher levels,[65,66] we transfected a low amount (0.5 μg) of either plasmid. This minimized expression while maintaining a transfection efficiency of ~40–50%. Only cells that displayed normal mitochondrial morphology were imaged. MFN1–10xmyc and MFN2–16xmyc each localize to puncta (Fig. 8D) along mitochondria and displayed very similar staining patterns to each other and to ARL2 (Fig. 8E). When co-staining for endogenous ARL2 and either MFN1/2-myc, we found that the puncta appeared to be adjacent to each other. We also noted that the ARL2 signal often appeared as if sandwiched in between mitofusin puncta, and this pattern was true for both MFN1-myc and MFN2-myc. This adjacent staining pattern is consistent with the localization of ARL2 to the IMS and the myc tags on mitofusins on the outer membrane, facing cytosol. Further supporting this interpretation, SMAC-HA-GFP pixel intensities also appeared maximal in between MFN2-myc puncta, though SMAC-HA-GFP appeared diffuse and not punctate. MFN puncta also appeared to display the same periodicity as ARL2 puncta, as they typically were found adjacent to ARL2 puncta (Fig. 8E). This pattern of MFN-myc localization also was consistent across varying levels of MFN-myc expression. The punctate staining suggests that ARL2 and MFNs are concentrated in loci in the IMS or outer membrane, respectively, and that they share a physical proximity.

We also tested whether OPA1 aligned with ARL2 puncta along mitochondria in COS7 cells. We first examined endogenous OPA1 and found that OPA1 also formed puncta along mitochondria. However, OPA1 puncta repeat along mitochondria at less uniform, and thus different, intervals from ARL2 puncta. These OPA1 positive puncta also did not show any consistent spatial correlation with ARL2; *i.e.*, they appeared next to ARL2 puncta as well as in between ARL2 puncta. We next expressed OPA1-myc/his in COS7 cells, though it caused mitochondrial fragmentation in some cells and elongation in others. Staining of these COS7 cells with the myc antibody showed that OPA1-myc/his appeared similar to endogenous OPA1 staining, in that they displayed no obvious regularity in spacing and were not correlated with puncta that were positive for ARL2 by SIM (Fig. 8C).

Thus, we conclude that ARL2 and MFNs display a novel localization along mitochondria, each demonstrating punctate staining with a periodicity of ~0.4 μm. These were not observed for several other mitochondrial proteins, including those that should mark cristae (Complex V subunit α), the TOM complex, sites of mitochondrial fission, the MICOS complex, the matrix, or the soluble fraction in the IMS.

Discussion

We identify ARL2 as a novel regulator of mitochondrial fusion, acting from the IMS and capable of promoting fusion through a mitofusin-dependent pathway. The findings that dominant mutants with opposite effects on ARL2 activity have opposing effects on mitochondrial morphology support a role for ARL2 in regulating mitochondrial fusion. We show that ARL2[T30N] causes mitochondrial fragmentation as a result of a reduction in the rate of fusion and that expression of ARL2[Q70L] leads to elongation of mitochondria with increased fusion. By targeting ARL2 constructs to different sub-mitochondrial compartments or to the cytosol, we show that its effects on mitochondrial morphology are most evident when directed to the IMS. By either targeting ARL2 to mitochondria or using a second site mutation that prevents effects on microtubules, we show that effects on mitochondria are independent of the previously documented effects of ARL2 mutants on microtubules. The finding that expression of ARL2[Q70L] is sufficient to partially restore fusion in MEFs deleted for either MFN1 or MFN2, but not both, is consistent with ARL2 promoting fusion in a fashion that requires at least one mitofusin. Using SIM, we also discovered that ARL2 localizes to discrete, regularly-spaced puncta along mitochondria that present a spatial convergence to staining of mitofusins. The mitofusins are also punctate in appearance, with very similar spacing and proximity to ARL2. This is in marked contrast to staining observed for several other markers of known mitochondrial complexes. Thus, we speculate that there exists a novel protein complex involved in fusion that includes at least ARL2 and mitofusins.

Our observations reveal that increasing or decreasing ARL2 activity using dominant mutations influences mitochondrial morphology in opposite ways. Expression of ARL2[T30N] causes mitochondrial fragmentation and the loss of fusion (Fig. 1). In contrast, expression of ARL2[Q70L] promotes mitochondrial elongation and increased fusion (Fig. 2). These data provide strong support for a role for ARL2 in the regulation of mitochondrial morphology. These dominant mutants are homologous to those used extensively in ARF family and RAS superfamily research. Our observations that the activating mutant of ARL2 promotes fusion and that the inactivating mutant causes fragmentation, as a result of a decrease in the rate of fusion, are completely consistent with a model in which ARL2 acts as a classical regulatory GTPase to regulate fusion.

The fact that the 2 mutants use different mechanisms, and act on targets either upstream or downstream of ARL2, can lead to differences in the kinetics of associated phenotypes. This is particularly true of the dominant negative mutant, ARL2[T30N], which is expressed to lower levels and more rapidly lost in cells. Despite this, it is more rapidly imported into mitochondria than the wild type or dominant activating mutant (Fig. 3). The fact that the ARL2 GAP, ELMOD2,[38,67-69] also localizes to mitochondria and that its knockdown causes mitochondrial fragmentation and loss of motility[38] also support our model that ARL2 is acting in mitochondria as a canonical regulatory GTPase.

Because inhibition of mitochondrial fission can mimic activation of fusion, and *vice versa*, it can be difficult to clearly distinguish mechanisms and pathways for regulators. We now believe that we misinterpreted our earlier experiments that depended solely upon expression of a dominant negative mutant of DRP1[38]. Expression of DRP1[K38A] reverses mitochondrial fragmentation observed in *mfn1*$^{-/-}$ or *mfn2*$^{-/-}$ MEFs (which have impaired rates of fusion (5)), but has no effect in *mfn1*$^{-/-}$*mfn2*$^{-/-}$ or *opa1*$^{-/-}$ MEFs (which have no fusion activity (4)). Consistent with such studies, the reversal we observed with DRP1[K38A] may have been caused by ongoing fusion in ARL2[T30N] cells over the course of our experiment, even though those cells had lower rates of fusion compared with controls. To test this possibility, we measured fusion by monitoring the rate of mito-PAGFP spreading throughout the mitochondrial network over a much shorter (40 min) time window, as previously documented and characterized.[43,44,70,71] Expression of ARL2[T30N] dramatically slowed the spread of mito-PAGFP (Fig. 1), while expression of ARL2[Q70L] increased it (Fig. 7D, E). These data strongly link increased ARL2 activity with increases in mitochondrial fusion and decreased ARL2 activity with a decreased rate of fusion. They are also consistent with our previous observation that depletion of ARL2 via siRNA causes fragmentation.[38] Though our results lead us to propose that ARL2 promotes fusion, we cannot completely exclude the possibility that it also can impact mitochondrial fission.

To begin to address the mechanism by which ARL2 can alter mitochondrial fusion, we must first dissect these novel effects from previously established roles for ARL2 in regulating tubulin and microtubules.[28,30-32,34,72-75] Based upon fractionation of cultured cells and mammalian tissues, we have estimated that only ~5–10% of cellular ARL2 is found in mitochondria. The vast majority of ARL2 is in the cytosol, complexed to the tubulin chaperone cofactor D (TBCD), or at centrosomes.[30,33,34,39] There are several other proteins with roles outside of mitochondria acting on different pathways inside mitochondria, including STAT3,[76,77] MEF2D,[78] fumarase,[79] several DNA repair proteins,[80] and others.[79,81-85] Nevertheless, when studying a protein with multiple cellular roles (the term "moonlighting roles" is increasingly used), it is important to resolve the different actions to allow functional and mechanistic studies of each. This can be particularly challenging when essential cellular functions are involved or when the 2 actions may yield similar phenotypes. Because movement of mitochondria along microtubules can facilitate fusion, we used multiple approaches to resolve effects of ARL2 on mitochondrial morphology from those on microtubules.

We were initially able to separate the effects of ARL2[T30N] from mitochondrial temporally, because mitochondrial phenotypes resulting from expression of ARL2[T30N] occurred 24 hours after transfection, whereas the microtubule effects did not appear until 48 hours after transfection.[38] However, the more overt phenotypes (loss of microtubules, changes in mitochondrial morphology or motility) may be late manifestations of earlier, more subtle changes. To better discriminate effects of ARL2 on mitochondria from those on microtubules, we identified 2 mutations ([L3A] and [F50A]) which disrupt its binding to TBCD and prevent its effects on microtubules.[33] In that earlier study, we found that [L3A] or [F50A] nearly completely eliminated both binding to TBCD and the effects on microtubules in cells, when combined with the activating [Q70L] mutation.[33] In marked contrast, when we assayed ARL2[L3A, Q70L] or ARL2[F50A, Q70L] for effects on mitochondria, we found that they all caused mitochondrial elongation to a similar extent as ARL2[Q70L] (Fig. 2), despite their inability to alter microtubules. This is taken as very strong evidence that effects of ARL2 on mitochondria cannot be purely secondary to effects on microtubules or tubulin. In addition, during the course of identifying the site of action of ARL2 on mitochondrial morphology, we used MLS leaders that strongly drove the fusion protein to different mitochondrial compartments. When we targeted ARL2[T30N] or ARL2[Q70L] to the IMS using the SMAC MLS, we found that each had comparable activity to the untagged mutant in altering mitochondrial dynamics (Figs. 5 and 7), with no effects on microtubules (Fig. 7C). Using either SMAC-HA-ARL2[Q70L] (Fig. 7A,D,E) or ARL2[F50A, Q70L] (Fig. 7D,E), we were able to preserve microtubules and show that dominant activating ARL2 stimulates fusion in *mfn2*$^{-/-}$ MEFs using the mito-PAGFP assay (Fig. 7D,E) to a similar extent as wild type ARL2, which has no effect on microtubules.[33,34] Therefore, we believe that we have cleanly resolved the effects of ARL2 on mitochondrial fusion from those on microtubules and have also developed important tools for others wishing to study the mitochondrial functions of ARL2.

To return to the question of mechanism by which ARL2 can alter mitochondrial fusion, we investigated its site of action. We used N-terminal fusions of previously characterized MLSs to drive ARL2 to different compartments and assess consequences to mitochondrial morphology. We show that ARL2[T30N] most readily causes mitochondrial fragmentation when targeted to the IMS. Only SMAC-HA-ARL2[T30N] was able to cause mitochondrial fragmentation to a similar extent as untagged ARL2[T30N]. The observations that SMAC-HA-ARL2 did not cause fragmentation, and that SMAC-HA-ARL2[T30N] still was able to promote fragmentation when expressed from a greatly weakened CMV promoter, CMVΔ6[61], supports the conclusion that fragmentation is not due to saturation of the IMS or mitochondrial import system. This conclusion is further strengthened by the observation that while the wild type and [Q70L] mutant proteins are expressed to comparable levels, ARL2[T30N] is always found at lower levels due to its relative instability, resulting from its decreased affinity for guanine nucleotides. Similarly, CMVΔ6 SMAC-HA-ARL2[Q70L] promoted elongation to a similar extent as untagged ARL2

[Q70L] (Fig. 7). Therefore, we conclude that ARL2 acts from the IMS to promote mitochondrial fusion.

We found that addition of even a small epitope tag to the N-terminus (Fig. 4) or deletion of the N-terminal 9 residues of ARL2 (unpublished observation) prevents its import into mitochondria. We also show that 2 different point mutants in the N-terminus result in loss of a subset of ARL2 functions.[33] From these data, we conclude that the N-terminus is involved in both mitochondrial import and acts as a third GTP-sensitive "switch" for this GTPase, comparable to the canonical switch I and II in all regulatory GTPases.[86] This conclusion is consistent with the use of N-terminal amphipathic helices (a hallmark of members of the ARF family of regulatory GTPases[87,88]) serving as mitochondrial import sequences[89-91] and X-ray crystal structures that show the ARL2 N-terminus binds directly to effectors.[54,55] In a related manuscript,[40] we provide further evidence that the fraction of cellular ARL2 at mitochondria changes in response to stressors. We currently lack details of the mechanism(s) by which ARL2 import is regulated, though we speculate that changes in localization provide the cell a means of communication between different essential processes, *e.g.*, mitotic spindle formation and energy metabolism.

With the evidence that ARL2 can alter fusogenic activities in cells, we turned to MEFs as a model due to the availability of several lines with different gene deletions. Remarkably, expression of ARL2[Q70L] reverses fragmentation resulting from the loss of either MFN1 or MFN2, but not both. We interpret these data as evidence that ARL2 can increase the activity of either mitofusin to promote fusion, but it requires at least one mitofusin to act. The promotion of outer membrane fusion by mitofusins involves both *cis*-oligomerization (by proteins in one mitochondrial outer membrane) as well as MFN-MFN binding in *trans*.[92] The kinetics of reversal varied between the different MEF lines, with reversal in *mfn2*$^{-/-}$ MEFs observed at 24 hours after transfection and gone by 48 hours, while reversal of fragmentation in *mfn1*$^{-/-}$ MEFs was more delayed, optimal at 48 hrs. Given that the same plasmid is used for reversal of each, we believe that this difference in kinetics is a reflection of the previously described[92] differences in fusogenic properties of MFN1 and MFN2. While the 2 proteins share 60% identity[93] and a level of functional redundancy, they differ in that MFN2 has additional metabolic roles[4, 94-97] and plays a role in mitochondria/ER tethering,[98] though this is contested.[99,100] The fusion activity of MFN1, still present in the *mfn2*$^{-/-}$ MEFs, is probably higher than that of MFN2, as evidenced by the higher percentage of cells with tubular morphology in *mfn2*$^{-/-}$ MEFs (26%) compared with *mfn1*$^{-/-}$ MEFs (0%). This is also consistent with MFN1 having better tethering and fusion activity *in vitro*.[92] We speculate that the higher fusogenic activity of MFN1 over that of MFN2 in MEFs also explains our result that overexpression of wild type ARL2 was able to partially reverse fragmentation in *mfn2*$^{-/-}$, but not *mfn1*$^{-/-}$ MEFs. ARL2 [Q70L] was unable to reverse fragmentation in *mfn1*$^{-/-}$*mfn2*$^{-/-}$ MEFs, demonstrating that fusion/elongation mediated by ARL2[Q70L] is dependent on the presence of a mitofusin, as previously shown for mitochondrial fusion in general.[4] ARL2 [Q70L] was also unable to reverse fragmentation in *opa1*$^{-/-}$ MEFs. The lack of reversal by ARL2 in either *mfn1*$^{-/-}$*mfn2*$^{-/-}$ or *opa1*$^{-/-}$ MEFs is consistent with these cells having absolutely no fusion activity, in contrast to *mfn1*$^{-/-}$ and *mfn2*$^{-/-}$ MEFs which retain some fusion activity.[4,5] Both the reversal of fragmentation and increase in mito-PAGFP spread in *mfn2*$^{-/-}$ MEFs are consistent with the interpretation that ARL2 reverses fragmentation in *mfn2*$^{-/-}$ MEFs by stimulating a mitofusin-dependent pathway. To the best of our knowledge, only 2 other proteins reverse fragmentation when expressed in either *mfn1*$^{-/-}$ or *mfn2*$^{-/-}$ MEFs (besides the mitofusins themselves, and DRP1[K38A], which blocks fission[5]). Expression of Bax restores tubular morphology in *mfn1*$^{-/-}$ but not *mfn2*$^{-/-}$ MEFs,[19] and expression of OPA1 causes elongation in *mfn2*$^{-/-}$ but not *mfn1*$^{-/-}$ MEFs.[6] Therefore, ARL2 is unique not only in that it can reverse fragmentation in these MEFs, but that it can do so through a pathway that includes either MFN1 or MFN2. Elongation induced by ARL2[Q70L] is also distinct from the previously described stress-induced mitochondrial hyperfusion (SIMH)[14] as ARL2[Q70L]-mediated elongation occurs in both *mfn2*$^{-/-}$ and *mfn1*$^{-/-}$ MEFs, whereas SIMH can occur in *mfn2*$^{-/-}$ but not *mfn1*$^{-/-}$ MEFs. Additionally, proteolytic cleavage of OPA1 is observed during SIMH, and we detect no changes in OPA1 processing with expression of ARL2[Q70L] We conclude that increasing ARL2 activity can lead to increased fusogenic activity of mitochondria through a mechanism that requires the canonical fusogens, MFN1/2, and OPA1.

In the hopes of better refining the localization of ARL2 in mitochondria, we used the higher resolution capabilities of SIM. We showed that ARL2 and mitofusins localize to puncta along mitochondria displaying regularity in spacing, while 9 other mitochondrial proteins, including those that localize to the matrix, the IMS, the inner membrane, or the outer membrane, do not. Most proteins displayed diffuse staining along mitochondria (TOM20, cytochrome C, HSP60, BART, SMAC-GFP), while those in puncta (DRP1, MFF, OPA1) did not show any clear relationship to ARL2. MICOS puncta, previously observed by STED microscopy,[101] repeat at a much smaller interval than 0.4 μm and were difficult to identify by SIM. Double labeling of endogenous ARL2 and MFN-myc showed ARL2 puncta commonly adjacent to and between MFN-myc puncta. We believe this observation is consistent with ARL2 associating with specific components accessible to it in the IMS, most likely at the outer membrane. Because we observed puncta that were positive for mitofusins and displayed both the same regularity in spacing as ARL2 and appeared adjacent to ARL2, we speculate that there exists a novel complex at which both ARL2 and mitofusins are found. MFN2 puncta have been described previously, and mutation of a residue involved in nucleotide binding disrupts this localization[102] During apoptosis, MFN2 forms puncta that co-localize with Bax and DRP1[103] These observations support the idea that mitofusins may contribute to one or more complexes along the outer membrane. We believe that there is functional significance to the close spatial pairing of MFN-myc and ARL2 puncta in such a putative structure, though we currently lack direct evidence to support such a conclusion. Further studies are planned to develop and test this hypothesis.

To summarize, we provide evidence that ARL2 can regulate mitochondrial fusion from the IMS and that it requires the presence in cells of at least one of the 2 mitofusins and OPA1. The only other proteins implicated in regulating fusion from

the IMS are proteases embedded in the inner membrane that cleave OPA1.[21-24] The little that was described previously about regulation of mitofusins occurs from the cytosol and outer membrane. Our data provide preliminary support for the existence of a novel structure or protein complex that contains at a minimum ARL2 and mitofusins and that may serve as the site of fusion coordination or nucleation. Further study of ARL2 and this putative protein complex will build upon these observations and help define the molecular mechanisms of mitochondrial fusion and its regulation in health and disease.

Experimental procedures

Antibodies & reagents

Rabbit polyclonal antibody directed against human ARL2 has been described previously.[39] The following antibodies were purchased: HA (Covance MMS-101P), HSP60 (Enzo Life Sciences ADI-SPA-807), cytochrome C (BD Biosciences 556432), TOM20 (BD Biosciences 61228), α-tubulin (Sigma T9026), myc (Invitrogen R950–25), OPA1 (BD Biosciences 612606), Complex V subunit α (Mitosciences MS502), NDUFA9 (Mitosciences MS111), UQCRC2 (Mitosciences MS304), actin (Sigma A3853).

Cloning and constructs

The following plasmids were generously gifted: MFN1–10xmyc and MFN2–16xmyc in pcDNA3.1 (David Chan, Caltech, (5)), OPA1-myc/his in pcDNA3.1 (Heidi McBride, McGill), mito-PAGFP (Richard Youle, NIH, Addgene plasmid #23348,[70]), mito-dsRed (James Zheng, Emory), GFP-MFF (Gia Voeltz, University of Colorado, Addgene plasmid #49153[104]), DRP1-YFP (Alexa Mattheyses, Emory). ARL2, ARL2[T30N], and ARL2[Q70L] in pcDNA3.1 were described previously.[34] [F50A] and [L3A] mutations were introduced into ARL2 [Q70L] in pcDNA3.1 using QuickChange (Stratagene) and sequence-verified. CMVΔ0 OCT-HA-ARL2 and CMVΔ0 SMAC-HA-ARL2 were also made in our laboratory as described previously Newman et al.[60]

Cell culture

Cells were grown in DMEM supplemented with 10% fetal bovine serum (Invitrogen, Carlsbad, CA) and 2 mM glutamine at 37°C in the presence of 5% CO_2. Cells were originally obtained from the ATCC and are not cultured beyond 30 passages. Cell density, feeding, and plating schedules were identical between all conditions in every experiment, with a target of 70% cell density for data collection. Wild type and *mfn1*$^{-/-}$, *mfn2*$^{-/-}$, *mfn1*$^{-/-}$*mfn2*$^{-/-}$, *opa1*$^{-/-}$ MEFs were a generous gift from David Chan (California Institute of Technology).[5,24,63] Cells were screened for mycoplasma regularly by staining with Hoechst 33342 DNA dye, usually in conjunction with immunofluorescence experiments (described below).

Transfection

Cells at 90% density or higher were transfected in 6 well plates using the following protocols. Both the amount of DNA and the ratio of Lipofectamine: DNA were separately optimized for ARL2 expression in HeLa and COS7 cells. A ratio of 2 μg Lipofectamine: 1 μg DNA yielded the highest transfection efficiency. ARL2 plasmids (2 μg) were diluted in 250 μL Opti-MEM (Invitrogen). Lipofectamine 2000 (4 μg; Invitrogen) was diluted in a separate tube containing 250 μL Opti-MEM, vortexed briefly, and incubated at room temperature for 5 minutes. The tubes were mixed and incubated 20 minutes. Cell culture medium was changed to 1.5 ml of Opti-MEM, and transfection complexes (500 μL) were added dropwise to the cells. After 4 hours, cells were trypsinized and replated onto coverslips, typically at a 1:3 split. For time points of 48 hours or longer after transfection, fresh medium (1 mL) was added before addition of transfection complexes, and the transfection was allowed to go for 24 hours, after which cells were typically split 1:4 onto coverslips. In both cases, cells were allowed to attach overnight before fixation. This transfection typically resulted in ~70% of cells overexpressing ARL2 and ~50% expressing ARL2[T30N] or ARL2[Q70L] when assayed 48 hours from the start of transfection.

MEFs were transfected using a similar protocol, though we found optimal ARL2 expression was obtained using a 3:1 ratio: 15 μg Lipofectamine 2000 and 5 μg DNA per well. Following transfection, cells were replated 1:4 (*mfn1*$^{-/-}$, *mfn2*$^{-/-}$) or 1:2 (*mfn1*$^{-/-}$*mfn2*$^{-/-}$, *opa1*$^{-/-}$) onto coverslips such that MEFs were at ~90% confluence the next day. This protocol typically resulted in ~40% of MEFs expressing MFN1-myc or MFN2-myc, ~20% expressing ARL2, ~10% expressing ARL2[Q70L], and 1–5% expressing OPA1-myc/his, as determined by immunofluorescence imaging of fixed cells. These differences are likely the result of differences in protein expression and antibody sensitivities rather than plasmid uptake. Slightly lower (~10–20%) transfection efficiencies were observed in *mfn1*$^{-/-}$*mfn2*$^{-/-}$ and *opa1*$^{-/-}$ MEFs, perhaps related to their increased doubling time and increased susceptibility to stress.

Immunofluorescence

Cells were grown on matrigel (BD Biosciences #356231) coated coverslips. Cells were fixed in a pre-warmed (37°C) solution of 4% paraformaldehyde in PBS (140 mM NaCl, 3 mM KCl, 10 mM Na_2HPO_4, 2 mM KH_2PO_4, pH 6.75); and permeabilized with 0.1% (v/v) Triton X-100 in PBS for 10 minutes at room temperature. Alternatively, cells were permeabilized with either 0.02% or 0.1% (w/v) digitonin in PBS for 10 minutes at room temperature to differentially permeabilize the outer and inner mitochondrial membrane, respectively, as described previously[105,106] For labeling of mitochondria with Mitotracker, cells were incubated in MitoTracker Red CMXRos (100 nM, Thermo Fisher #M7512) for 30 minutes before fixation. Incubation with primary antibodies was performed in filtered PBS containing 1% (w/v) BSA at 4°C overnight, followed by 4 × 5 minute washes in PBS. Secondary antibodies (1:500, Alexa fluorophores, Invitrogen) were incubated in the same buffer for 1 hour at room temperature, following 4 × 5 minute washes in PBS. Secondary antibody was removed by 2 × 5 minute washes in PBS. DNA was then stained with Hoechst 33342 for 4 minutes, followed by 2 × 5 minutes washes in PBS and mounting onto slides using Prolong Antifade (Invitrogen). Images were acquired using an Olympus FV1000 microscope

and Olympus Fluoview v1.7 software, using 488 and 543 laser excitation and a 100x oil objective (1.45 NA). Z-stacks were acquired with a step size of 0.37 μm, which were converted to average image intensity projections using ImageJ where indicated. The following antibody dilutions were used: ARL2 (1:2000), HSP60 (1:5000), myc (1:1000), HA (1:2000), TOM20 (1:5000), cytochrome C (1:1000), α tubulin (1:2000), OPA1 (1:100), NDUFA9 [Complex I] (1:100), UQCRC2 [Complex III] (1:100), Complex V subunit α (1:100).

Effects of protein expression on mitochondrial morphology were scored by visual inspection of fixed, stained cells. To quantify consequences of protein expression on mitochondrial morphology in MEFs, the following categories were used: 1) Fragmented = mitochondria appear spherical with no long or branched structures evident, 2) short tubes = mitochondria appear shorter than in wild type controls but not spherical and show minimal interconnectivity, 3) tubular = mitochondria appear long and thread-like, with branching. Examples of each of these are shown in Figure S2. A cell was assigned to a category if an estimated 50% or more of its mitochondria fit one of these descriptions, as described previously.[19] For quantification of elongation in HeLa cells, we used the following categories: 1) elongated = the majority of mitochondria appear interconnected and individual mitochondria are difficult to discern, 2) tubular = individual mitochondria are easily discernable but the majority are not fragmented, 3) fragmented = most mitochondria appear small and spherical. A cell was excluded from analysis if it appeared to be dying, as defined by cell rounding with membrane blebs and fragmented nuclear staining; these cells typically had the highest levels of expression in the cell population. Only transfected cells were scored, and were identified as follows: 1) ARL2 over-expressing cells were identified by ARL2 staining (ARL2 staining appears obviously brighter than surrounding cells in the field) or 2) MFN1/2-myc by detectible mitochondrial myc staining.

Live cell imaging

HeLa cells were transfected with 0.5 μg mito-PAGFP, 0.25 μg mito-dsRed, and 2 μg of either ARL2 WT or ARL2[T30N], and replated onto 35 mm MatTek dishes (#P35GC-1.5–14-C) following 4 hours of transfection, as described above. For experiments in *mfn2*$^{-/-}$ MEFs, cells were transfected with 2 μg mito-PAGFP, 1 μg mito-dsRed, and 3 μg of the indicated plasmid. Prior to imaging, the medium was changed to DMEM with 25 mM HEPES plus 10% FBS, and without phenol red (Invitrogen #21063). Live cell imaging was performed using a Nikon A1R confocal microscope, enclosed in a temperature control chamber at 37°C, using a 100X (NA 1.49) oil objective. A circular region of interest (4 μm diameter) for photoactivation was selected near the nucleus.[71] Photoactivation was achieved by excitation with 405 nm laser (35% power) for 6 cycles for a total duration of 2.16 seconds. Images were acquired at 1024 × 1024 pixels at 0.5 frames/second during photoactivation. Images were then acquired every 10 minutes over 40 minutes. GFP and dsRed were sequentially excited with 488 and 561 laser lines. Imaging data were collected using Nikon Elements software. Quantification of the mito-PAGFP mitochondrial fusion assay was performed as described previously[44] using ImageJ. A cell was excluded from analysis if it 1) had less than a 10-fold increase in GFP signal following photoactivation, or 2) moved from the field of view during imaging. In addition, only cells with fragmented mitochondria were selected when imaging cells transfected with ARL2 [T30N]. Masks for each channel were created, and thresholding was performed using "Otsu dark" in ImageJ. The number of pixels within each mask for both GFP and dsRed was measured, and calculated as a ratio of GFP signal to dsRed signal. The difference in this ratio between 0 min. (immediately after photoactivation) and 10, 20, 30, or 40 min. after photoactivation is reported as percent increase in mitochondrial fusion.

Structured Illumination Microscopy (SIM)

For SIM experiments, the minimal amount of transfected DNA was determined for each construct for both optimal expression and minimal effects on mitochondrial morphology. COS7 cells were transfected with 0.5 μg MFN1-myc, MFN2-myc, or 2 μg of OPA1-myc/his. A ratio of 2 μg Lipofectamine 2000: 1 μg DNA was used for all constructs. Cells were imaged on a Nikon N-SIM using 3-dimensional SIM using a 100X (NA 1.49) oil objective. Cells were selected based on an apparently normal mitochondrial morphology, and a range of expression for each construct was examined. Fluorophores were excited by 488 and 561 laser lines. For each cell, a widefield image was obtained in addition to raw SIM data. Reconstruction was achieved using the Nikon Elements software, and reconstruction parameters suggested by the software were adjusted with reference to the widefield image, to avoid described previously artifacts (for examples see http://www.gelifesciences.com/gehcls_images/GELS/Pdf%20documents/2015–05–06-Pellett-Bitesizebio-Seminar.pdf).

Mitochondrial fractionation

Mitochondria were fractionated using a previously published protocol[107] Cells were washed twice in PBS, incubated for 10 minutes in 5 mM EDTA in PBS, and collected. Cells were pelleted and washed in TD buffer (25 mM Tris-HCl, pH 7.4, 0.7 mM Na_2HPO_4, 133 mM NaCl, 5 mM KCl). Cells were resuspended in RSB buffer (10 mM Tris-HCl pH 7.4, 10 mM NaCl, 1.5 mM $CaCl_2$, protease inhibitors (Sigma #P-2714)), to a final volume of about 10x the volume of the cell pellet, and incubated on ice for 10 minutes before homogenization with a Dounce glass/glass tight homogenizer (30 strokes). Lysis of cells was verified using trypan blue. MS buffer, prepared as a 2.5X stock, was added to yield a final concentration of 1x MS (5 mM Tris-HCl pH 7.4, 210 mM mannitol, 70 mM sucrose, 5 mM EDTA pH 8). Unbroken cells and nuclei were removed by centrifugation (10 min., 1000xg), after which mitochondria were pelleted from the post-nuclear supernatant (20 min., 14,000xg).

Western blotting

Cells were harvested by rinsing twice with PBS, collected by incubation in 5 mM EDTA in phosphate buffered saline (PBS; 140 mM NaCl, 3 mM KCl, 10 mM Na2HPO4, 2 mM KH2PO4, pH 6.75), and pelleted in a microfuge (14,000 rpm, 4°C). Cells

were lysed in 1% CHAPS, 25 mM HEPES pH 7.4, 100 mM NaCl, and protease inhibitors (Sigma #P-2714) on ice for 30 minutes, and the S14 was obtained by clarifying lysates by centrifugation for 30 minutes (14,000 rpm, 4°C). Protein concentrations were determined by Bradford Assay (Bio-Rad) using bovine serum albumin as standard. Protein samples (20 μg/well) were separated on 15% polyacrylamide gels and wet-transferred to nitrocellulose membranes (Bio-Rad #162–0112) at 70V for 2.5 hours. Western blotting procedures were performed at room temperature. Membranes were blocked in blotto (5% (w/v) dry milk, 50 mM Tris pH 8, 2 mM $CaCl_2$, 80 mM NaCl, 0.2% (v/v) Tween-20, 0.02% sodium azide) for 1 hour. When probing for ARL2, membranes were blocked in an alternate blocking buffer (10% goat serum, 5% Tween-20 in PBS), freshly filtered through a 0.2 μm membrane. Membranes were then incubated with primary antibody in blocking buffer at 4°C overnight. Removal of excess primary antibody was performed by washing the membranes in PBST (PBS with 0.1% Tween-20) 3 times for 10 min each. HRP-conjugated secondary antibodies (GE cat #NA934V, #NA931V) were diluted 1:5000 in PBST and incubated with the membrane for 1 hour at room temperature. Excess secondary antibody was removed by washing the membranes in PBST 3 times for 10 min each. Excess Tween-20 was removed by quickly rinsing membranes 3 times in PBS, followed by 2 × 5 minute washes in PBS. Blots were incubated in luminol containing solution (0.1 mM Tris-HCl pH 8.0, 1.2 mM luminol, 0.2 mM p-coumaric acid, 0.009% hydrogen peroxide) for 1 min before exposure to film. The following antibody dilutions were used for western blotting: ARL2 (1:1000), α tubulin (1:2500), actin (1:2000), OPA1 (1:1000). For blotting of OCT or SMAC-HA-ARL2, data were instead collected using the Odyssey Infrared Imager, and membranes were incubated in anti-rabbit 790 secondary antibody (Invitrogen A11374) or anti-mouse 800 secondary antibody (Rockland 610–745–002), diluted 1:10,000 in PBST. Immunoblotting with antibodies to α tubulin or actin was performed in each case as a loading control to confirm equal total protein loaded per lane, in agreement with total protein assays.

Reproducibility

Every experiment described has been independently repeated at least twice. For quantification of immunofluorescence experiments, experiments were independently repeated at least 3 times, and at least 200 cells per condition were analyzed per experiment. Error bars represent standard error of the mean (SEM).

Abbreviations

ARL2	ADP-ribosylation factor-like 2
BN-PAGE	blue native polyacrylamide gel electrophoresis
DRP1	dynamin related protein 1
IMS	intermembrane space
MFN1/2	mitofusin 1/2
mito-PAGFP	mitochondria targeted photoactivatable GFP
MLS	mitochondria localization sequence
OCT	ornithine carbamoyltransferase (or the 32 residue leader sequence derived from the human protein)
OPA1	optic atrophy 1
SEM	standard error of the mean
SIM	structured illumination microscopy.
SMAC	(second mitochondria-derived activator of caspases, or the 59 residue leader sequence derived from the human protein; aka Diablo)

Disclosure of potential conflicts of interest

No potential conflicts of interest were disclosed.

Acknowledgments

We thank Drs. David Chan (Caltech), Heidi McBride (McGill), Richard Youle (NIH), James Zheng (Emory), Gia Voeltz (University of Colorado), and Alexa Mattheyses (Emory) for their generous gift of plasmids. We thank Dr. Alexa Mattheyses, Laura Fox-Goharioon, and Neil Anthony of the Integrated Cellular Imaging (ICI) core at Emory University for assistance with obtaining and analyzing imaging data.

Funding

This research was supported in part by the Emory University Integrated Cellular Imaging Microscopy Core of the Emory Neuroscience NINDS Core Facilities grant, P30NS055077. This work was supported by grants from the National Institutes of Health 5R01GM090158 to RAK and 1F31GM111047 to LEN, and an American Heart Association pre-doctoral fellowship 14PRE18840040 to LEN. The content is solely the responsibility of the authors and does not necessarily represent the official views of the National Institutes of Health.

Author contributions

LEN, CRS, and RET designed, performed, and analyzed experiments. LEN and CRS prepared the figures. LEN and RAK designed the study and wrote the paper, with input from CRS and RET. All authors reviewed the results and approved the final version of the manuscript.

References

[1] Labrousse AM, Zappaterra MD, Rube DA, van der Bliek AM. C. elegans dynamin-related protein DRP-1 controls severing of the mitochondrial outer membrane. Mol Cell 1999; 4:815-26; PMID:10619028; https://doi.org/10.1016/S1097-2765(00)80391-3

[2] Smirnova E, Griparic L, Shurland DL, van der Bliek AM. Dynamin-related protein Drp1 is required for mitochondrial division in mammalian cells. Mol Biol Cell 2001; 12:2245-56; PMID:11514614; https://doi.org/10.1091/mbc.12.8.2245

[3] Mishra P, Chan DC. Mitochondrial dynamics and inheritance during cell division, development and disease. Nat Rev Mol Cell Biol 2014; 15:634-46; PMID:25237825; https://doi.org/10.1038/nrm3877

[4] Chen H, Chomyn A, Chan DC. Disruption of fusion results in mitochondrial heterogeneity and dysfunction. J Biol Chem 2005; 280:26185-92; PMID:15899901; https://doi.org/10.1074/jbc.M503062200

[5] Chen H, Detmer SA, Ewald AJ, Griffin EE, Fraser SE, Chan DC. Mitofusins Mfn1 and Mfn2 coordinately regulate mitochondrial fusion and are essential for embryonic development. J Cell Biol 2003; 160:189-200; PMID:12527753; https://doi.org/10.1083/jcb.200211046

[6] Cipolat S, de Brito OM, Dal Zilio B, Scorrano L. OPA1 requires mitofusin 1 to promote mitochondrial fusion. Proc Natl Acad Sci U S A 2004; 101:15927-32; PMID:15509649; https://doi.org/10.1073/pnas.0407043101

[7] Griparic L, van der Wel NN, Orozco IJ, Peters PJ, van der Bliek AM. Loss of the intermembrane space protein Mgm1/OPA1 induces swelling and localized constrictions along the lengths of

mitochondria. J Biol Chem 2004; 279:18792-8; PMID:14970223; https://doi.org/10.1074/jbc.M400920200

[8] Zuchner S, Mersiyanova IV, Muglia M, Bissar-Tadmouri N, Rochelle J, Dadali EL, Zappia M, Nelis E, Patitucci A, Senderek J, et al. Mutations in the mitochondrial GTPase mitofusin 2 cause charcot-marie-tooth neuropathy type 2A. Nat Genet 2004; 36:449-51; PMID:15064763; https://doi.org/10.1038/ng1341

[9] Delettre C, Lenaers G, Griffoin JM, Gigarel N, Lorenzo C, Belenguer P, Pelloquin L, Grosgeorge J, Turc-Carel C, Perret E, et al. Nuclear gene OPA1, encoding a mitochondrial dynamin-related protein, is mutated in dominant optic atrophy. Nat Genet 2000; 26:207-10; PMID:11017079; https://doi.org/10.1038/79936

[10] Alexander C, Votruba M, Pesch UE, Thiselton DL, Mayer S, Moore A, Rodriguez M, Kellner U, Leo-Kottler B, Auburger G, et al. OPA1, encoding a dynamin-related GTPase, is mutated in autosomal dominant optic atrophy linked to chromosome 3q28. Nat Genet 2000; 26:211-5; PMID:11017080; https://doi.org/10.1038/79944

[11] Chen H, McCaffery JM, Chan DC. Mitochondrial fusion protects against neurodegeneration in the cerebellum. Cell 2007; 130:548-62; PMID:17693261; https://doi.org/10.1016/j.cell.2007.06.026

[12] Gomes LC, Di Benedetto G, Scorrano L. During autophagy mitochondria elongate, are spared from degradation and sustain cell viability. Nat Cell Biol 2011; 13:589-98; PMID:21478857; https://doi.org/10.1038/ncb2220

[13] Rambold AS, Kostelecky B, Elia N, Lippincott-Schwartz J. Tubular network formation protects mitochondria from autophagosomal degradation during nutrient starvation. Proc Natl Acad Sci U S A 2011; 108:10190-5; PMID:21646527; https://doi.org/10.1073/pnas.1107402108

[14] Tondera D, Grandemange S, Jourdain A, Karbowski M, Mattenberger Y, Herzig S, Da Cruz S, Clerc P, Raschke I, Merkwirth C, et al. SLP-2 is required for stress-induced mitochondrial hyperfusion. EMBO J 2009; 28:1589-600; PMID:19360003; https://doi.org/10.1038/emboj.2009.89

[15] Mishra P, Carelli V, Manfredi G, Chan DC. Proteolytic cleavage of Opa1 stimulates mitochondrial inner membrane fusion and couples fusion to oxidative phosphorylation. Cell Metab 2014; 19:630-41; PMID:24703695; https://doi.org/10.1016/j.cmet.2014.03.011

[16] Song Z, Ghochani M, McCaffery JM, Frey TG, Chan DC. Mitofusins and OPA1 mediate sequential steps in mitochondrial membrane fusion. Mol Biol Cell 2009; 20:3525-32; PMID:19477917; https://doi.org/10.1091/mbc.E09-03-0252

[17] Chan DC. Fusion and fission: interlinked processes critical for mitochondrial health. Annu Rev Genet 2012; 46:265-87; PMID:22934639; https://doi.org/10.1146/annurev-genet-110410-132529

[18] Chen H, Vermulst M, Wang YE, Chomyn A, Prolla TA, McCaffery JM, Chan DC. Mitochondrial fusion is required for mtDNA stability in skeletal muscle and tolerance of mtDNA mutations. Cell 2010; 141:280-9; PMID:20403324; https://doi.org/10.1016/j.cell.2010.02.026

[19] Hoppins S, Edlich F, Cleland MM, Banerjee S, McCaffery JM, Youle RJ, Nunnari J. The soluble form of Bax regulates mitochondrial fusion via MFN2 homotypic complexes. Mol Cell 2011; 41:150-60; PMID:21255726; https://doi.org/10.1016/j.molcel.2010.11.030

[20] Eura Y, Ishihara N, Oka T, Mihara K. Identification of a novel protein that regulates mitochondrial fusion by modulating mitofusin (Mfn) protein function. Journal of Cell Science 2006; 119:4913-25; PMID:17105775; https://doi.org/10.1242/jcs.03253

[21] Griparic L, Kanazawa T, van der Bliek AM. Regulation of the mitochondrial dynamin-like protein Opa1 by proteolytic cleavage. J Cell Biol 2007; 178:757-64; PMID:17709430; https://doi.org/10.1083/jcb.200704112

[22] Head B, Griparic L, Amiri M, Gandre-Babbe S, van der Bliek AM. Inducible proteolytic inactivation of OPA1 mediated by the OMA1 protease in mammalian cells. J Cell Biol 2009; 187:959-66; PMID:20038677; https://doi.org/10.1083/jcb.200906083

[23] Ehses S, Raschke I, Mancuso G, Bernacchia A, Geimer S, Tondera D, Martinou JC, Westermann B, Rugarli EI, Langer T. Regulation of OPA1 processing and mitochondrial fusion by m-AAA protease isoenzymes and OMA1. J Cell Biol 2009; 187:1023-36; PMID:20038678; https://doi.org/10.1083/jcb.200906084

[24] Song Z, Chen H, Fiket M, Alexander C, Chan DC. OPA1 processing controls mitochondrial fusion and is regulated by mRNA splicing, membrane potential, and Yme1L. J Cell Biol 2007; 178:749-55; PMID:17709429; https://doi.org/10.1083/jcb.200704110

[25] Clark J, Moore L, Krasinskas A, Way J, Battey J, Tamkun J, Kahn RA. Selective amplification of additional members of the ADP-ribosylation factor (ARF) family: cloning of additional human and Drosophila ARF-like genes. Proc Natl Acad Sci U S A 1993; 90:8952-6; PMID:8415637; https://doi.org/10.1073/pnas.90.19.8952

[26] Li Y, Kelly WG, Logsdon JM, Jr, Schurko AM, Harfe BD, Hill-Harfe KL, Kahn RA. Functional genomic analysis of the ADP-ribosylation factor family of GTPases: phylogeny among diverse eukaryotes and function in C. elegans. FASEB J 2004; 18:1834-50; https://doi.org/10.1096/fj.04-2273com

[27] Antoshechkin I, Han M. The C. elegans evl-20 gene is a homolog of the small GTPase ARL2 and regulates cytoskeleton dynamics during cytokinesis and morphogenesis. Dev Cell 2002; 2:579-91; PMID:12015966; https://doi.org/10.1016/S1534-5807(02)00146-6

[28] Radcliffe PA, Vardy L, Toda T. A conserved small GTP-binding protein Alp41 is essential for the cofactor-dependent biogenesis of microtubules in fission yeast. FEBS Lett 2000; 468:84-8; PMID:10683446; https://doi.org/10.1016/S0014-5793(00)01202-3

[29] McElver J, Patton D, Rumbaugh M, Liu C, Yang LJ, Meinke D. The TITAN5 gene of Arabidopsis encodes a protein related to the ADP ribosylation factor family of GTP binding proteins. Plant Cell 2000; 12:1379-92; PMID:10948257; https://doi.org/10.1105/tpc.12.8.1379

[30] Shern JF, Sharer JD, Pallas DC, Bartolini F, Cowan NJ, Reed MS, Pohl J, Kahn RA. Cytosolic Arl2 is complexed with cofactor D and protein phosphatase 2A. J Biol Chem 2003; 278:40829-36; PMID:12912990; https://doi.org/10.1074/jbc.M308678200

[31] Bhamidipati A, Lewis SA, Cowan NJ. ADP ribosylation factor-like protein 2 (Arl2) regulates the interaction of tubulin-folding cofactor D with native tubulin. J Cell Biol 2000; 149:1087-96; PMID:10831612; https://doi.org/10.1083/jcb.149.5.1087

[32] Tian G, Thomas S, Cowan NJ. Effect of TBCD and its regulatory interactor Arl2 on tubulin and microtubule integrity. Cytoskeleton (Hoboken) 2010; 67:706-14; PMID:20740604; https://doi.org/10.1002/cm.20480

[33] Francis JW, Newman LE, Cunningham LA, Kahn RA. A trimer consisting of the tubulin-specific chaperone D (TBCD), regulatory GTPase ARL2, and beta-Tubulin Is required for maintaining the microtubule network. J Biol Chem 2017; 292:4336-49; PMID:28126905; https://doi.org/10.1074/jbc.M116.770909

[34] Zhou C, Cunningham L, Marcus AI, Li Y, Kahn RA. Arl2 and Arl3 regulate different microtubule-dependent processes. Mol Biol Cell 2006; 17:2476-87; PMID:16525022; https://doi.org/10.1091/mbc.E05-10-0929

[35] Cunningham LA, Kahn RA. Cofactor D functions as a centrosomal protein and is required for the recruitment of the gamma-tubulin ring complex at centrosomes and organization of the mitotic spindle. J Biol Chem 2008; 283:7155-65; PMID:18171676; https://doi.org/10.1074/jbc.M706753200

[36] Ismail SA, Chen YX, Rusinova A, Chandra A, Bierbaum M, Gremer L, Triola G, Waldmann H, Bastiaens PIH, Wittinghofer A. Arl2-GTP and Arl3-GTP regulate a GDI-like transport system for farnesylated cargo. Nat Chem Biol 2011; 7:942-9; PMID:22002721; https://doi.org/10.1038/nchembio.686

[37] Fansa EK, Wittinghofer A. Sorting of lipidated cargo by the Arl2/Arl3 system. Small GTPases 2016; 7(4):222-30 1-9

[38] Newman LE, Zhou CJ, Mudigonda S, Mattheyses AL, Paradies E, Marobbio CM, Kahn RA. The ARL2 GTPase is required for mitochondrial morphology, motility, and maintenance of ATP levels. PloS One 2014; 9:e99270; PMID:24911211; https://doi.org/10.1371/journal.pone.0099270

[39] Sharer JD, Shern JF, Van Valkenburgh H, Wallace DC, Kahn RA. ARL2 and BART enter mitochondria and bind the adenine

nucleotide transporter. Mol Biol Cell 2002; 13:71-83; PMID:11809823; https://doi.org/10.1091/mbc.01-05-0245

[40] Newman LE, Schiavon CR, Zhou C, Kahn RA. Recruitment of the ARL2 GTPase and its GAP, ELMOD2, to Mitochondria is Modulated by the Fusogenic Activity of Mitofusins. PloS One 2017; 12(4): e0175164 In press; https://doi.org/10.1371/journal.pone.0175164

[41] Karbowski M, Arnoult D, Chen H, Chan DC, Smith CL, Youle RJ. Quantitation of mitochondrial dynamics by photolabeling of individual organelles shows that mitochondrial fusion is blocked during the Bax activation phase of apoptosis. J Cell Biol 2004; 164:493-9; PMID:14769861; https://doi.org/10.1083/jcb.200309082

[42] Karbowski M, Cleland MM, Roelofs BA. Photoactivatable green fluorescent protein-based visualization and quantification of mitochondrial fusion and mitochondrial network complexity in living cells. Methods Enzymol 2014; 547:57-73; PMID:25416352

[43] Anand R, Wai T, Baker MJ, Kladt N, Schauss AC, Rugarli E, Langer T. The i-AAA protease YME1L and OMA1 cleave OPA1 to balance mitochondrial fusion and fission. J Cell Biol 2014; 204:919-29; PMID:24616225; https://doi.org/10.1083/jcb.201308006

[44] Zunino R, Braschi E, Xu L, McBride HM. Translocation of SenP5 from the Nucleoli to the Mitochondria Modulates DRP1-dependent Fission during Mitosis. J Biol Chem 2009; 284:17783-95; PMID:19411255; https://doi.org/10.1074/jbc.M901902200

[45] Ichishita R, Tanaka K, Sugiura Y, Sayano T, Mihara K, Oka T. An RNAi screen for mitochondrial proteins required to maintain the morphology of the organelle in Caenorhabditis elegans. J Biochem 2008; 143:449-54; PMID:18174190; https://doi.org/10.1093/jb/mvm245

[46] Zhang CJ, Rosenwald AG, Willingham MC, Skuntz S, Clark J, Kahn RA. Expression of a dominant allele of human ARF1 inhibits membrane traffic in vivo. J Cell Biol 1994; 124:289-300; PMID:8294513; https://doi.org/10.1083/jcb.124.3.289

[47] Van Valkenburgh H, Shern JF, Sharer JD, Zhu X, Kahn RA. ADP-ribosylation factors (ARFs) and ARF-like 1 (ARL1) have both specific and shared effectors: characterizing ARL1-binding proteins. J Biol Chem 2001; 276:22826-37; PMID:11303027; https://doi.org/10.1074/jbc.M102359200

[48] Scheffzek K, Ahmadian MR, Kabsch W, Wiesmuller L, Lautwein A, Schmitz F, Wittinghofer A. The Ras-RasGAP complex: structural basis for GTPase activation and its loss in oncogenic Ras mutants. Science 1997; 277:333-8; PMID:9219684; https://doi.org/10.1126/science.277.5324.333

[49] Der CJ, Finkel T, Cooper GM. Biological and biochemical properties of human rasH genes mutated at codon 61. Cell 1986; 44:167-76; PMID:3510078; https://doi.org/10.1016/0092-8674(86)90495-2

[50] Hobbs GA, Der CJ, Rossman KL. RAS isoforms and mutations in cancer at a glance. J Cell Sci 2016; 129:1287-92; PMID:26985062; https://doi.org/10.1242/jcs.182873

[51] Hanzal-Bayer M, Linari M, Wittinghofer A. Properties of the interaction of Arf-like protein 2 with PDEdelta. J Mol Biol 2005; 350:1074-82; PMID:15979089; https://doi.org/10.1016/j.jmb.2005.05.036

[52] Joneson T, White MA, Wigler MH, Bar-Sagi D. Stimulation of membrane ruffling and MAP kinase activation by distinct effectors of RAS. Science 1996; 271:810-2; PMID:8628998; https://doi.org/10.1126/science.271.5250.810

[53] Kuai J, Boman AL, Arnold RS, Zhu X, Kahn RA. Effects of activated ADP-ribosylation factors on Golgi morphology require neither activation of phospholipase D1 nor recruitment of coatomer. J Biol Chem 2000; 275:4022-32; PMID:10660559; https://doi.org/10.1074/jbc.275.6.4022

[54] Hanzal-Bayer M, Renault L, Roversi P, Wittinghofer A, Hillig RC. The complex of Arl2-GTP and PDE delta: from structure to function. EMBO J 2002; 21:2095-106; PMID:11980706; https://doi.org/10.1093/emboj/21.9.2095

[55] Zhang T, Li S, Zhang Y, Zhong C, Lai Z, Ding J. Crystal structure of the ARL2-GTP-BART complex reveals a novel recognition and binding mode of small GTPase with effector. Structure 2009; 17:602-10; PMID:19368893; https://doi.org/10.1016/j.str.2009.01.014

[56] Horwich AL, Kalousek F, Fenton WA, Pollock RA, Rosenberg LE. Targeting of pre-ornithine transcarbamylase to mitochondria: Definition of critical regions and residues in the leader peptide. Cell 1986; 44:451-9; PMID:3943133; https://doi.org/10.1016/0092-8674(86)90466-6

[57] Horwich AL, Kalousek F, Mellman I, Rosenberg LE. A leader peptide is sufficient to direct mitochondrial import of a chimeric protein. EMBO J 1985; 4:1129-35; PMID:3891325

[58] Ozawa T, Natori Y, Sako Y, Kuroiwa H, Kuroiwa T, Umezawa Y. A minimal peptide sequence that targets fluorescent and functional proteins into the mitochondrial intermembrane space. ACS Chem Biol 2007; 2:176-86; PMID:17348629; https://doi.org/10.1021/cb600492a

[59] Sabharwal SS, Waypa GB, Marks JD, Schumacker PT. Peroxiredoxin-5 targeted to the mitochondrial intermembrane space attenuates hypoxia-induced reactive oxygen species signalling. Biochem J 2013; 456:337-46; PMID:24044889; https://doi.org/10.1042/BJ20130740

[60] Newman LE, Schiavon C, Kahn RA. Plasmids for variable expression of proteins targeted to the mitochondrial matrix or intermembrane space. Cell Logistics 2016; 6:e1247939; PMID:28042516; https://doi.org/10.1080/21592799.2016.1247939

[61] Morita E, Arii J, Christensen D, Votteler J, Sundquist WI. Attenuated protein expression vectors for use in siRNA rescue experiments. Biotechniques 2012; 0:1-5; PMID:22877307

[62] Cipolat S, Martins de Brito O, Dal Zilio B, Scorrano L. OPA1 requires mitofusin 1 to promote mitochondrial fusion. Proc Natl Acad Sci U S A 2004; 101:15927-32; PMID:15509649; https://doi.org/10.1073/pnas.0407043101

[63] Koshiba T, Detmer SA, Kaiser JT, Chen H, McCaffery JM, Chan DC. Structural basis of mitochondrial tethering by mitofusin complexes. Science 2004; 305:858-62; PMID:15297672; https://doi.org/10.1126/science.1099793

[64] Rojo M, Legros F, Chateau D, Lombès A. Membrane topology and mitochondrial targeting of mitofusins, ubiquitous mammalian homologs of the transmembrane GTPase Fzo. J Cell Sci 2002; 115:1663-74; PMID:11950885

[65] Eura Y, Ishihara N, Yokota S, Mihara K. Two mitofusin proteins, mammalian homologues of FZO, with distinct functions are both required for mitochondrial fusion. J Biochem 2003; 134:333-44; PMID:14561718; https://doi.org/10.1093/jb/mvg150

[66] Santel A, Fuller MT. Control of mitochondrial morphology by a human mitofusin. J Cell Sci 2001; 114:867-74; PMID:11181170

[67] Bowzard JB, Cheng D, Peng J, Kahn RA. ELMOD2 is an Arl2 GTPase-activating protein that also acts on Arfs. J Biol Chem 2007; 282:17568-80; PMID:17452337; https://doi.org/10.1074/jbc.M701347200

[68] Ivanova AA, East MP, Yi SL, Kahn RA. Characterization of recombinant ELMOD (cell engulfment and motility domain) proteins as GTPase-activating proteins (GAPs) for ARF family GTPases. J Biol Chem 2014; 289:11111-21; PMID:24616099; https://doi.org/10.1074/jbc.M114.548529

[69] East MP, Bowzard JB, Dacks JB, Kahn RA. ELMO domains, evolutionary and functional characterization of a novel GTPase-activating protein (GAP) domain for Arf protein family GTPases. J Biol Chem 2012; 287:39538-53; PMID:23014990; https://doi.org/10.1074/jbc.M112.417477

[70] Karbowski M, Arnoult D, Chen H, Chan DC, Smith CL, Youle RJ. Quantitation of mitochondrial dynamics by photolabeling of individual organelles shows that mitochondrial fusion is blocked during the Bax activation phase of apoptosis. J Cell Biol 2004; 164:493-9; PMID:14769861; https://doi.org/10.1083/jcb.200309082

[71] Karbowski M, Cleland MM, Roelofs BA. Chapter four - photoactivatable green fluorescent protein-based visualization and quantification of mitochondrial fusion and mitochondrial network complexity in living cells. in Methods in Enzymology (NM Anne, and CC David eds.), Academic Press. pp 57-73, 2014

[72] Steinborn K, Maulbetsch C, Priester B, Trautmann S, Pacher T, Geiges B, Kuttner F, Lepiniec L, Stierhof YD, Schwarz H, et al. The Arabidopsis PILZ group genes encode tubulin-folding cofactor orthologs required

for cell division but not cell growth. Genes Dev 2002; 16:959-71; PMID:11959844; https://doi.org/10.1101/gad.221702

[73] Tzafrir I, McElver JA, Liu Cm CM, Yang LJ, Wu JQ, Martinez A, Patton DA, Meinke DW. Diversity of TITAN functions in Arabidopsis seed development. Plant Physiol 2002; 128:38-51; PMID:11788751; https://doi.org/10.1104/pp.010911

[74] Beghin A, Honore S, Messana C, Matera EL, Aim J, Burlinchon S, Braguer D, Dumontet C. ADP ribosylation factor like 2 (Arl2) protein influences microtubule dynamics in breast cancer cells. Exp Cell Res 2007; 313:473-85; PMID:17188265; https://doi.org/10.1016/j.yexcr.2006.10.024

[75] Price HP, Peltan A, Stark M, Smith DF. The small GTPase ARL2 is required for cytokinesis in Trypanosoma brucei. Mol Biochem Parasitol 2010; 173:123-31; PMID:20653091; https://doi.org/10.1016/j.molbiopara.2010.05.016

[76] Gough DJ, Corlett A, Schlessinger K, Wegrzyn J, Larner AC, Levy DE. Mitochondrial STAT3 supports Ras-dependent oncogenic transformation. Science 2009; 324:1713-6; PMID:19556508; https://doi.org/10.1126/science.1171721

[77] Wegrzyn J, Potla R, Chwae YJ, Sepuri NB, Zhang Q, Koeck T, Derecka M, Szczepanek K, Szelag M, Gornicka A, et al. Function of mitochondrial Stat3 in cellular respiration. Science 2009; 323:793-7; PMID:19131594; https://doi.org/10.1126/science.1164551

[78] She H, Yang Q, Shepherd K, Smith Y, Miller G, Testa C, Mao Z. Direct regulation of complex I by mitochondrial MEF2D is disrupted in a mouse model of Parkinson disease and in human patients. J Clin Invest 2011; 121:930-40; PMID:21393861; https://doi.org/10.1172/JCI43871

[79] Yogev O, Naamati A, Pines O. Fumarase: a paradigm of dual targeting and dual localized functions. FEBS J 2011; 278:4230-42; PMID:21929734; https://doi.org/10.1111/j.1742-4658.2011.08359.x

[80] Bauer NC, Corbett AH, Doetsch PW. The current state of eukaryotic DNA base damage and repair. Nucleic Acids Res 2015; 43:10083-101; PMID:26519467

[81] Bauer NC, Doetsch PW, Corbett AH. Mechanisms regulating protein localization. Traffic 2015; 16:1039-61; PMID:26172624; https://doi.org/10.1111/tra.12310

[82] Ackema KB, Hench J, Bockler S, Wang SC, Sauder U, Mergentaler H, Westermann B, Bard F, Frank S, Spang A. The small GTPase Arf1 modulates mitochondrial morphology and function. EMBO J 2014; 33:2659-75; PMID:25190516; https://doi.org/10.15252/embj.201489039

[83] Li CC, Wu TS, Huang CF, Jang LT, Liu YT, You ST, Liou GG, Lee FJ. GTP-binding-defective ARL4D alters mitochondrial morphology and membrane potential. PLoS One 2012; 7:e43552; PMID:22927989; https://doi.org/10.1371/journal.pone.0043552

[84] Regev-Rudzki N, Yogev O, Pines O. The mitochondrial targeting sequence tilts the balance between mitochondrial and cytosolic dual localization. J Cell Sci 2008; 121:2423-31; PMID:18577574; https://doi.org/10.1242/jcs.029207

[85] Petrungaro C, Riemer J. Mechanisms and physiological impact of the dual localization of mitochondrial intermembrane space proteins. Biochem Soc Trans 2014; 42:952-8; PMID:25109985; https://doi.org/10.1042/BST20140104

[86] Sprang SR. G protein mechanisms: insights from structural analysis. Annu Rev Biochem 1997; 66:639-78; PMID:9242920; https://doi.org/10.1146/annurev.biochem.66.1.639

[87] Amor JC, Horton JR, Zhu X, Wang Y, Sullards C, Ringe D, Cheng X, Kahn RA. Structures of yeast ARF2 and ARL1: distinct roles for the N terminus in the structure and function of ARF family GTPases. J Biol Chem 2001; 276:42477-84; PMID:11535602; https://doi.org/10.1074/jbc.M106660200

[88] Amor JC, Harrison DH, Kahn RA, Ringe D. Structure of the human ADP-ribosylation factor 1 complexed with GDP. Nature 1994; 372:704-8; PMID:7990966; https://doi.org/10.1038/372704a0

[89] Hartl FU, Neupert W. Import of proteins into the various submitochondrial compartments. J Cell Sci Suppl 1989; 11:187-98; PMID:2559090; https://doi.org/10.1242/jcs.1989.Supplement_11.15

[90] Neupert W. Protein import into mitochondria. Annu Rev Biochem 1997; 66:863-917; PMID:9242927; https://doi.org/10.1146/annurev.biochem.66.1.863

[91] Neupert W, Herrmann JM. Translocation of proteins into mitochondria. Annu Rev Biochem 2007; 76:723-49; PMID:17263664; https://doi.org/10.1146/annurev.biochem.76.052705.163409

[92] Ishihara N, Eura Y, Mihara K. Mitofusin 1 and 2 play distinct roles in mitochondrial fusion reactions via GTPase activity. J Cell Sci 2004; 117:6535-46; PMID:15572413; https://doi.org/10.1242/jcs.01565

[93] Santel A, Frank S, Gaume B, Herrler M, Youle RJ, Fuller MT. Mitofusin-1 protein is a generally expressed mediator of mitochondrial fusion in mammalian cells. J Cell Sci 2003; 116:2763-74; PMID:12759376; https://doi.org/10.1242/jcs.00479

[94] Pich S, Bach D, Briones P, Liesa M, Camps M, Testar X, Palacin M, Zorzano A. The Charcot-Marie-Tooth type 2A gene product, Mfn2, up-regulates fuel oxidation through expression of OXPHOS system. Hum Mol Genet 2005; 14:1405-15; PMID:15829499; https://doi.org/10.1093/hmg/ddi149

[95] Bach D, Pich S, Soriano FX, Vega N, Baumgartner B, Oriola J, Daugaard JR, Lloberas J, Camps M, Zierath JR, et al. Mitofusin-2 determines mitochondrial network architecture and mitochondrial metabolism. A novel regulatory mechanism altered in obesity. J Biol Chem 2003; 278:17190-7

[96] Mourier A, Motori E, Brandt T, Lagouge M, Atanassov I, Galinier A, Rappl G, Brodesser S, Hultenby K, Dieterich C, et al. Mitofusin 2 is required to maintain mitochondrial coenzyme Q levels. J Cell Biol 2015; 208:429-42; PMID:25688136; https://doi.org/10.1083/jcb.201411100

[97] Schrepfer E, Scorrano L. Mitofusins, from mitochondria to metabolism. Mol Cell 2016; 61:683-94; PMID:26942673; https://doi.org/10.1016/j.molcel.2016.02.022

[98] de Brito OM, Scorrano L. Mitofusin 2 tethers endoplasmic reticulum to mitochondria. Nature 2008; 456:605-10; PMID:19052620; https://doi.org/10.1038/nature07534

[99] Cosson P, Marchetti A, Ravazzola M, Orci L. Mitofusin-2 independent juxtaposition of endoplasmic reticulum and mitochondria: an ultrastructural study. PLoS One 2012; 7:e46293; PMID:23029466; https://doi.org/10.1371/journal.pone.0046293

[100] Filadi R, Greotti E, Turacchio G, Luini A, Pozzan T, Pizzo P. Mitofusin 2 ablation increases endoplasmic reticulum-mitochondria coupling. Proc Natl Acad Sci U S A 2015; 112:E2174-2181; PMID:25870285; https://doi.org/10.1073/pnas.1504880112

[101] Jans DC, Wurm CA, Riedel D, Wenzel D, Stagge F, Deckers M, Rehling P, Jakobs S. STED super-resolution microscopy reveals an array of MINOS clusters along human mitochondria. Proc Natl Acad Sci U S A 2013; 110:8936-41; PMID:23676277; https://doi.org/10.1073/pnas.1301820110

[102] Neuspiel M, Zunino R, Gangaraju S, Rippstein P, McBride H. Activated mitofusin 2 signals mitochondrial fusion, interferes with Bax activation, and reduces susceptibility to radical induced depolarization. J Biol Chem 2005; 280:25060-70; PMID:15878861; https://doi.org/10.1074/jbc.M501599200

[103] Karbowski M, Lee YJ, Gaume B, Jeong SY, Frank S, Nechushtan A, Santel A, Fuller M, Smith CL, Youle RJ. Spatial and temporal association of Bax with mitochondrial fission sites, Drp1, and Mfn2 during apoptosis. J Cell Biol 2002; 159:931-8; PMID:12499352; https://doi.org/10.1083/jcb.200209124

[104] Friedman JR, Lackner LL, West M, DiBenedetto JR, Nunnari J, Voeltz GK. ER tubules mark sites of mitochondrial division. Science 2011; 334:358-62; PMID:21885730; https://doi.org/10.1126/science.1207385

[105] Jeyaraju DV, Xu L, Letellier MC, Bandaru S, Zunino R, Berg EA, McBride HM, Pellegrini L. Phosphorylation and cleavage of presenilin-associated rhomboid-like protein (PARL) promotes changes in mitochondrial morphology. Proc Natl Acad Sci U S A 2006; 103:18562-7; PMID:17116872; https://doi.org/10.1073/pnas.0604983103

[106] Otera H, Ohsakaya S, Nagaura Z, Ishihara N, Mihara K. Export of mitochondrial AIF in response to proapoptotic stimuli depends on processing at the intermembrane space. EMBO J 2005; 24:1375-86; PMID:15775970; https://doi.org/10.1038/sj.emboj.7600614

[107] Tapper DP, Van Etten RA, Clayton DA. Isolation of mammalian mitochondrial DNA and RNA and cloning of the mitochondrial genome. Methods Enzymol 1983; 97:426-34; PMID:6197614